

HYPERBOLIC AWARE MINIMIZATION: IMPLICIT BIAS FOR SPARSITY

Tom Jacobs Advait Gadhikar Celia Rubio-Madrigal Rebekka Burkholz
 CISPA Helmholtz Center for Information Security, Saarbrücken, Germany
 {tom.jacobs, burkholz}@cispa.de

ABSTRACT

Understanding the implicit bias of optimization algorithms is key to explaining and improving the generalization of deep models. The hyperbolic implicit bias induced by pointwise overparameterization promotes sparsity, but also yields a small inverse Riemannian metric near zero, slowing down parameter movement and impeding meaningful parameter sign flips. To overcome this obstacle, we propose Hyperbolic Aware Minimization (HAM), which alternates a standard optimizer step with a lightweight hyperbolic mirror step. The mirror step incurs less compute and memory than pointwise overparameterization, reproduces its beneficial hyperbolic geometry for feature learning, and mitigates the small-inverse-metric bottleneck. Our characterization of the implicit bias in the context of underdetermined linear regression provides insights into the mechanism how HAM consistently increases performance—even in the case of dense training, as we demonstrate in experiments with standard vision benchmarks. HAM is especially effective in combination with different sparsification methods, advancing the state of the art.

1 INTRODUCTION

The success of modern deep learning relies on large amounts of overparameterization, which has led to a computationally demanding trend to increase the size of models, and thus the number of trainable parameters by orders of magnitude (Hoffmann et al., 2022; Kaplan et al., 2020). A common explanation for this phenomenon are implicit biases that originate from a combination of the optimizer and the overparameterization (Pesme et al., 2021; Gunasekar et al., 2017a; Woodworth et al., 2020), which regularize the training dynamics and thus improve the generalization performance.

Training sparse models instead leads to suboptimal performance (Li et al., 2017; Frankle & Carbin, 2018). This fact has limited pruning at initialization (PaI) approaches (Tanaka et al., 2020; Lee et al., 2019; Liu et al., 2021a) that aim to reduce the heavy computational and memory demands by masking the network before training the remaining parameters. In contrast, state-of-the-art sparsification methods utilize overparameterization in some capacity, as they either gradually prune parameters in Dense-to-Sparse (DtS) training (Peste et al., 2021; Kuznedelev et al., 2024; Kusupati et al., 2020; Jacobs & Burkholz, 2025; Kolb et al., 2025) or dynamically explore multiple sparse masks to find high-performing sparse networks with Dynamic Sparse Training (DST) (Evcı et al., 2020; Lasby et al., 2023; Chen et al., 2021). Key observations regarding these algorithms are that a) mild sparsity (which does not degrade performance relative to a dense baseline) (Jin et al., 2022) and b) longer training with standard optimizers can improve generalization performance significantly. The latter indicates that sparse models are difficult to train and take longer to converge (Kuznedelev et al., 2023). Consequently, sparse training ideally leverages overparameterization to improve generalization.

A recent development to improve sparse training is the pointwise overparameterization proposed in PILoT (Jacobs & Burkholz, 2025) and Sign-In (Gadhikar et al., 2025). All parameter weights $\theta \in \mathbb{R}^n$ are replaced by a pointwise product of parameters $m \odot w$, with both $m, w \in \mathbb{R}^n$. This changes the implicit bias of the optimization process and leads to substantial generalization benefits for sparse training. In PILoT, a continuous sparsification method, the overparameterization is used to jointly learn the mask m . Meanwhile, the PaI method Sign-In uses it to increase the plasticity of non-masked parameters and facilitate sign flips, which was shown to be a major obstacle in sparse training (Gadhikar & Burkholz, 2024a). Both methods, PILoT and Sign-In, achieve state-of-the-art

	Implicit sparsity bias	Sign flips	No hard perturbations	No extra parameters
Dense training	✗	—	✓	✓
PILoT (Jacobs & Burkholz, 2025)	✓	✗	✓	✗
Sign-In (Gadhikar et al., 2025)	✓ (less strong)	✓	✗	✗
HAM (ours)	✓ (less strong)	✓	✓	✓

Table 1: HAM induces a less strong implicit sparsity bias (moderating between L_2 and L_1) and flips parameter signs more easily due to its inverse metric (see Fig. 1), which together lead to boosting sparse training without explicit overparameterization.

results in their respective categories. However, on their own, they fall short of baseline methods of sparse training that do not utilize this form of overparameterization, such as AC/DC (Peste et al., 2021) and RiGL (Evci et al., 2020). To understand this gap, we investigate their training dynamics.

The dynamics of the overparameterization $m \odot w$ can be derived within the mirror flow (Li et al., 2022) or time-dependent mirror flow framework (Jacobs et al., 2025). It is associated with the hyperbolic mirror map (Woodworth et al., 2020) and, depending on initialization, learning rate, and regularization, it changes from an implicit L_2 (Dense) to L_1 (Sparse) bias during training. The mirror flow induced by $m \odot w$ can also be characterized by a Riemannian gradient flow with an associated metric (Li et al., 2022). Comparing these metrics highlights a problem: $m \odot w$ suffers from a small inverse metric $g^{-1}(\theta)$ near the origin, where g is a Riemannian metric tensor (Jacobs & Burkholz, 2025) (see Fig. 1 and Appendix F). As a consequence, parameters can get stuck at 0, preventing effective sign-flips. Sign-In partially mitigates this issue by iteratively re-initializing m and w such that $m \odot w$ remains fixed. We set $\gamma := (m^2 - w^2)^2 \gg 0$. However, the remedy is unstable and introduces a hard perturbation to the training dynamics, limiting its positive effects.

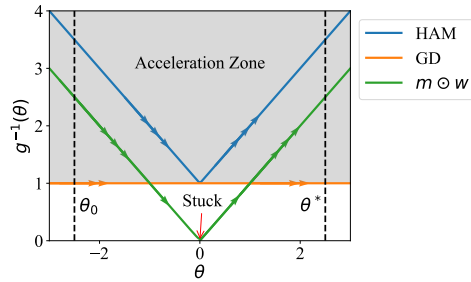


Figure 1: The inverse metric $g^{-1}(\theta)$ of HAM is above the one of gradient descent (GD), while the overparameterization $m \odot w$ is below for small γ . This enables moving from the initialization θ_0 to the optimum θ^* instead of getting stuck. Therefore, HAM fixes the vanishing inverse metric. Note the hyperbolic geometric structure of HAM and $m \odot w$ compared to the flatness of GD.

In this work, we propose to capture the essential structure of the two methods PILoT and Sign-In and thus the implicit bias of pointwise overparameterization $m \odot w$, which provably aids in finding generalizable sparse solutions. At the same time, we are able to avoid their drawbacks: their slow down near zero and their need for explicit overparameterization that negatively impacts memory and compute (see Table 1). We do this by deriving a plug-and-play hyperbolic optimization step, which we alternate with gradient descent or any other first-order optimizer. Our alternating method is called HAM: Hyperbolic Aware Minimization (§ 3, 3.1). HAM mitigates the small inverse metric problem of $m \odot w$ and keeps a similar but fully controllable implicit bias, as shown in § 4. We evaluate HAM on standard vision benchmarks and find that it consistently improves generalization, especially of sparse training (§ 5). Remarkably, HAM tends to enhance generalization complementary to sharpness aware minimization (SAM) (Foret et al., 2021), yet incurs only negligible computational overhead. These improvements can be explained by two major mechanisms: a) It accelerates training around 0, thus improving sign learning. This is facilitated by its geometry and a larger inverse metric. b) The implicit bias towards sparsity regularizes training inducing a mild sparsity. Both mechanisms boost generalization performance of sparsification techniques, such as AC/DC (Peste et al., 2021) and RiGL (Evci et al., 2020), and even of dense model training. In summary, our contributions are:

- We introduce HAM, a lightweight, plug-and-play general purpose optimization step that integrates with any optimizer at a negligible computational cost.
- We provide a theoretical analysis of HAM’s training dynamics using Riemannian gradient flow for linear regression (§ 4), characterizing its implicit bias and sign-flipping mechanism (Appendix E).

- HAM inherits the geometric benefits of recent sparsity parameterizations while mitigating their vanishing inverse metric problem (see Figure 1 and Appendix F). The benefits are an implicit sparsity bias which facilitates a mild sparsity and complementary sign flips to those of dense training.
- Empirically, HAM improves state-of-the-art sparsity methods (AC/DC, RiGL, STR), enhances standard dense training, and is also compatible with optimizers like SAM.

2 RELATED WORK

Sparsification Sparse training methods can be categorized into three broad classes: Pruning at Initialization (PaI), Dense-to-Sparse training (DtS), and Dynamic Sparse Training (DTS). PaI methods identify a sparse mask at initialization and train the remaining parameters to convergence. They include methods like SNIP (Lee et al., 2019), Synflow (Tanaka et al., 2020), NPB (Pham et al., 2023), PHEW (Patil & Dovrolis, 2021), GraSP (Wang et al., 2020) and random pruning (Liu et al., 2021a; Gadhikar et al., 2023). Their primary limitation is that standard optimizers do not find generalizable solutions on these fixed masks, as they struggle to effectively learn parameter signs (Gadhikar & Burkholz, 2024b; Gadhikar et al., 2025). In contrast, DtS methods learn the mask via a dense or denser phase of training, followed by any kind of pruning step and possibly more training. This includes iterative pruning methods like IMP (Frankle & Carbin, 2019), LRR (Renda et al., 2020; Han et al., 2015), AC/DC (Peste et al., 2021), CAP (Kuznedelev et al., 2024), and WoodFisher (Singh & Alistarh, 2020). Continuous sparsification methods, which start from a dense network and gradually sparsify it with a learnable mask, also fall under this category. They include PILoT (Jacobs & Burkholz, 2025), STR (Kusupati et al., 2020), CS (Savarese et al., 2021) and spread (Ziyin & Wang, 2022). The third class of methods, Dynamic Sparse Training, start from an already sparse mask but dynamically update it during training, and in this sense utilize a form of (dynamic) overparameterization (Liu et al., 2021b). Examples include RiGL (Evcı et al., 2020), MEST (Yuan et al., 2021), and SET (Mocanu et al., 2018). While PaI methods cannot compete with the generalization performance of DtS and DST methods, Sign-In (Gadhikar et al., 2025) improves on PaI by using the pointwise overparameterization $m \odot w$, which leverages a hyperbolic mirror map to facilitate sign flips. In this work, we propose instead a simpler, more powerful hyperbolic optimization step to leverage a similar mirror map without doubling the number of parameters and solving an issue with an associated inverse metric.

Implicit bias and mirror flow The implicit bias of neural networks is a well studied topic that aims to explain the regularization benefits resulting from overparameterization (Woodworth et al., 2020; Gunasekar et al., 2017b; 2018; Li et al., 2022). It is primarily characterized within the mirror flow framework, a well-established concept in convex optimization (Alvarez et al., 2004; Beck & Teboulle, 2003; Rockafellar & Fenchel, 1970; Boyd & Vandenberghe, 2009; Sun et al., 2022). A mirror flow can be seen as a gradient flow on a Riemannian manifold (Li et al., 2022; Alvarez et al., 2004) with the metric tensor being the Hessian of the Legendre function, which has also been extended to cover stochastic gradient descent (SGD) (Pesme et al., 2021; Even et al., 2023; Lyu & Zhu, 2023) and more recently to explicit regularization (Jacobs et al., 2025). This framework allows us to characterize the implicit bias. The main observation is that large learning rates, stochastic noise from SGD, and regularization can benefit generalization by implicitly inducing sparsity. However, overparameterization can also lead to small inverse metrics, slowing down convergence and potentially hampering generalization (Jacobs & Burkholz, 2025), which we can successfully avoid in HAM.

Related optimizers The mirror flow framework also enables us to view our algorithm HAM through the lens of natural gradient descent. Accordingly, the inverse metric is adapted due to (an approximation of) the Fisher information matrix, which captures second-order information (Martens, 2014; Amari, 1999). A more general Bayesian framework (Khan & Rue, 2021) has been used to gain insights into invariant distributions by using Lie groups (Kiral et al., 2023) and to develop the IVON optimizer (Shen et al., 2024). Within this framework, HAM, our proposal that alternates exponential updates with gradient descent steps, can be interpreted as a mapping of the Fisher information (metric) to a known posterior distribution, as derived in Appendix C. Moreover, our proposed hyperbolic update is reminiscent of exponentiated gradient descent (Kivinen & Warmuth, 1994). Distinctly from HAM, it optimizes probability distributions and thus includes normalization to stay on a probability simplex, as seen, for example, in Chapter 7 of Vishnoi (2021). Exponential gradient descent, which has recently been applied to reweighting batches (Majidi et al., 2021) or

augmenting ADAM (Bernstein et al., 2020), also utilizes similar exponential updates but does not rely on an alternating scheme like HAM. This prevents it from facilitating more suitable sign flips than gradient descent. More advantages of HAM are analyzed in Appendix D and E.

Two-step and alternating schemes Various previous works have explored alternating training schemes including proximal methods, soft thresholding, ADMM, alternating least squares, and expectation maximization, among others (Parikh & Boyd, 2014; Boyd et al., 2011; Cichocki et al., 2009; McLachlan & Krishnan, 1996). The most related alternating algorithms to HAM are based on birth-death dynamics at a neuron level in two-layer neural network training (Rotskoff et al., 2019) or variational inference (Mielke & Zhu, 2025; Gladin et al., 2024; Yan et al., 2024). An important difference is that we work on a weight level while other approaches work on a neuron or distribution level and serve an entirely different purpose. Furthermore, one of the most well-known two-step approaches is sharpness aware minimization (SAM) (Foret et al., 2021), which promotes the search for flat solutions at the expense of almost doubling the compute of one optimization step. In contrast, HAM encourages an implicit sparsity bias and acceleration around 0, which are complementary mechanisms. Our experiments (Table 3) demonstrate that our proposed hyperbolic step can be effectively combined with SAM to further boost generalization.

3 MOTIVATION AND DERIVATION OF HAM

We derive our novel optimization step by building on insights from the implicit bias of recently developed sparse training methods. These methods have exploited a reparameterization of the neural network: They replace each weight θ with a product of two weights $\mathbf{m} \odot \mathbf{w}$, where \odot is the Hadamard product, i.e., a pointwise multiplication. For this reparameterization, it is known that stochastic noise and weight decay induce sparsity by an implicit L_1 penalty (Pesme et al., 2021; Jacobs & Burkholz, 2025). The next paragraphs restate the induced gradient flow of this reparameterization (where the learning rate $\eta \rightarrow 0$). Note that \mathbf{u}^2 abbreviates $\mathbf{u} \odot^2$.

Gradient flow training Consider a continuously differentiable and L-smooth¹ loss function $f : \mathbb{R}^n \rightarrow \mathbb{R}$. It can be trained by means of gradient descent: $\theta_{k+1} = \theta_k - \eta \nabla f(\theta_k)$, initialized at $\theta_0 = \theta_{init}$, where $\eta > 0$ is the learning rate. Taking $\eta \rightarrow 0$, we obtain its gradient flow: $d\theta_t = -\nabla f(\theta_t) dt$. Its integral form is used in the mirror flow analysis and descriptions of the implicit bias: $\theta_t - \theta_0 = -\int_0^t \nabla f(\theta_s) ds$.

Reparameterized gradient flow Li et al. (2022) derive a similar formulation for the reparameterization $\mathbf{m} \odot \mathbf{w}$ trained with gradient descent, while Theorem 2.1 in Jacobs & Burkholz (2025) integrates weight decay with strength β in the analysis resulting of the following gradient flow:

$$\begin{cases} dm_t = -w_t \odot \nabla f(\theta_t) dt - 2\beta m_t dt, & w_0 = w_{init}, \\ dw_t = -m_t \odot \nabla f(\theta_t) dt - 2\beta w_t dt, & m_0 = m_{init}. \end{cases}$$

This corresponds to the integral equation for $\theta_t = \mathbf{m}_t \odot \mathbf{w}_t$:

$$\theta_t = \mathbf{u}_0^2 \odot \exp\left(-2 \int_0^t \nabla f(\theta_s) ds - 4\beta t\right) - \mathbf{v}_0^2 \odot \exp\left(2 \int_0^t \nabla f(\theta_s) ds - 4\beta t\right), \quad (1)$$

where $\mathbf{u}_0 := \frac{\mathbf{m}_0 + \mathbf{w}_0}{\sqrt{2}}$ and $\mathbf{v}_0 := \frac{\mathbf{m}_0 - \mathbf{w}_0}{\sqrt{2}}$ for $|\mathbf{w}_0| \leq \mathbf{m}_0$ are chosen such that $\mathbf{u}_0^2 - \mathbf{v}_0^2 = \theta_0$. $\beta > 0$ is the strength of weight decay. This results in a time varying Riemannian gradient flow for θ_t :

$$d\theta_t = \sqrt{\theta_t^2 + \gamma_t^2} \odot \nabla f(\theta_t) dt - 2\beta \theta_t dt, \quad \theta_0 = \theta_{init}, \quad (2)$$

where $\gamma_t = 4\mathbf{u}_0^2 \odot \mathbf{v}_0^2 \exp(-4\beta t)$. Eq. (2) implies that we cannot move through zero when $\gamma_t \rightarrow 0$.

Exponential gradient descent The hyperbolic gradient flow in Eq. (1) not only corresponds to the gradient flow of $\mathbf{m} \odot \mathbf{w}$, but also to exponential gradient descent. This is presented by Wu & Rebeschini (2021) for matrix forms in a matrix sensing task without regularization ($\beta = 0$). We use this connection to derive an update without the need for the reparameterization (or regularization). The update is captured by the following theorem:

¹See Definition A.1 in the appendix for a definition of L-smoothness.

Theorem 3.1 *If $m_0 = \text{sign}(\theta_0)w_0 = \sqrt{|\theta_0|}$, then*

$$\theta_{k+1} = \theta_k \exp(-\eta(2 \text{sign}(\theta_k)\nabla f(\theta_k) + 4\beta)) \quad (3)$$

is equivalent to Eq. (1) up to first order, i.e., the discretization error is $\mathcal{O}(\eta^2)$.

Proof. See proof of Theorem B.1 in the appendix. \square

Note that a more general update for a product of matrices is provided by Wu & Rebeschini (2021). Their exponential update suffers from the same problem as the parameterization $\mathbf{m} \odot \mathbf{w}$, as it corresponds to $\gamma = \mathbf{0}$ and thus completely preventing sign flips (see Corollary B.2). Our proposal HAM overcomes this obstacle by alternating a gradient step with an exponential update step.

Derivation of HAM The novelty stems from alternating the new hyperbolic update in Eq. (3) with another optimizer. This forms the basis of our proposal HAM. We derive its explicit form for gradient descent as follows:

$$\theta_{k+\frac{1}{2}} = \theta_k - \eta\nabla f(\theta_k), \quad (\text{GD})$$

$$\theta_{k+1} = \theta_{k+\frac{1}{2}} \odot \exp(-\eta(\alpha \text{sign}(\theta_k)\nabla f(\theta_k) + \beta)). \quad (\text{HYP})$$

Note it is not necessary to use the same learning rate for gradient descent and for the exponential update. In fact, the learning rates control the strength of the implicit bias towards sparsity, for which we have introduced an additional hyperparameter $\alpha \in \mathbb{R}$. The exponential update now more closely resembles the hyperbolic gradient update in Eq. (1), as it can switch the sign in the exponential. § 4 studies the resulting gradient flow.

Interpretation The exponential update (HYP) introduces a weight scaling which correspond to a metric $g(\theta) = 1/|\theta|$ for a Riemannian gradient flow, as we will see in §4. This changes how parameters evolve compared to standard gradient descent. When the sign of a parameter is correct, the update refines its magnitude. If the sign is incorrect, it drives the parameter exponentially fast toward zero. However, on its way to a sign flip, the parameter gets stuck in 0 —because the parameter update is proportional to $\theta = 0$ at the origin. To facilitate the sign flip, we need the intermediary gradient step (GD), which explains the advantages of HAM over pure exponential updates. In summary, our combined update can be interpreted as: *Learn the magnitude when the sign is correct; otherwise, move rapidly to zero to enable sign correction.* This mechanism is crucial for enabling sparse training (Gadhikar & Burkholz, 2024a; Gadhikar et al., 2025), as shown in our experiments (§ 5), where HAM significantly boosts performance compared to standard optimizers.

Remark 3.2 *Note that the second step (HYP) depends both on θ_k and $\theta_{k+\frac{1}{2}}$, which would require twice the memory of gradient descent. To avoid this, we replace $\text{sign}(\theta_k)$ with $\text{sign}(\theta_{k+\frac{1}{2}})$. We restate the second HAM step actually deployed (HYP*) in §3.1. It also has benefits for the optimization itself, promoting more stable sign flips, as we discuss in Appendix D and Figure 6. Building on recent work on sign flips (Gadhikar et al., 2025), we argue that the sign should be aligned with the gradient evaluation to assess whether the step should be accelerated or not, to promote meaningful sign flips. This insight is tightly linked to our choice of $\text{sign}(\theta_{k+\frac{1}{2}})$ instead of $\text{sign}(\theta_k)$ in the (HYP*) step.*

3.1 ALGORITHM: HYPERBOLIC AWARE MINIMIZATION (HAM)

We propose HAM (Algorithm 1), which alternates between any standard optimizer step and a hyperbolic (signed) mirror map to improve the general trainability of neural networks. The proposed method is inspired by recent sparsification methods, as theoretically justified in § 4. We next state the main algorithmic innovations.

Hyperbolic step Let $\eta > 0$ denote the learning rate and $\alpha, \beta \geq 0$ be positive constants. The hyperbolic step deployed with parameters $\theta_k \in \mathbb{R}^n$ is given by

$$\theta_k = \theta_{k+\frac{1}{2}} \odot \exp\left(-\eta\left(\alpha \text{sign}(\theta_{k+\frac{1}{2}})\nabla f(\theta_k) + \beta\right)\right), \quad (\text{HYP}^*)$$

where $\theta_{k+\frac{1}{2}}$ is the step of any other optimizer. α controls the convergence speed and hyperbolic awareness of the method, and β induces an explicit regularization similar to that of PILoT (Jacobs &

Algorithm 1 HAM

Require: steps T , schedule η , initialization θ_{init} , constants $\alpha, \beta \geq 0$.
for $k \in 0 \dots T - 1$ **do**
 $\theta_{k+\frac{1}{2}} = \text{OptimizerStep}(\nabla f(\theta_k), \eta)$
 $\theta_{k+1} = \text{HyperbolicStep}(\theta_{k+\frac{1}{2}}, \nabla f(\theta_k), \alpha, \beta, \eta)$ according to formula (HYP*)
end for
return Model weights θ_T

Burkholz, 2025). Note that we have replaced $\text{sign}(\theta_k)$ with $\text{sign}(\theta_{k+\frac{1}{2}})$, as mentioned in Remark 3.2. Our analysis of implicit bias § 4 still remains valid with this change, as we show in Appendix Theorem B.6.

Memory and compute overhead HAM does not incur any memory overhead, as it reuses the known gradient and current signs of the weights. In contrast, the pointwise overparameterization $m \odot w$ doubles the number of parameters, which would only be negligible in case of large batch sizes—where activations dominate the memory requirements (Ziyin & Wang, 2022; Jacobs & Burkholz, 2025; Kolb et al., 2025). Moreover, the additional extra flops during training are negligible, as they are linear in the number of parameters.

4 THEORY: GRADIENT FLOW ANALYSIS

Our theory (Eqs. (GD,HYP)) identifies the implicit bias of HAM’s Riemannian gradient flow in parameter space (Thm. 4.2) and provides a convergence analysis (Thms. 4.3 and 4.5). Accordingly, HAM solves the vanishing inverse metric problem of $m \odot w$, and thus converges faster, while retaining the same asymptotic implicit sparsity bias. In this section, we assume that the objective function $f : \mathbb{R}^n \rightarrow \mathbb{R}$ is continuously differentiable, i.e., $f \in C^1$, and L -smooth¹. Appendix E proves that HAM also induces meaningful sign flips like $m \odot w$ (Gadhikar et al., 2025). We focus on the case $\beta = 0$ to simplify the exposition. Theorem 4.2 derives the flow for general β . The effects of nonzero β are highlighted in Section B.1.

Riemannian gradient flows In order to concisely study the behavior of HAM, we consider a gradient flow formulation. Gradient flow (flat) and $m \odot w$ (hyperbolic) flow can be described as Riemannian gradient flows depending on a general metric $g(\theta)$:

$$d\theta_t = -g^{-1}(\theta_t)\nabla f(\theta_t)dt, \quad \theta_0 = \theta_{init}.$$

We refer to the quantity $g^{-1}(\theta)$ as the inverse metric. It is trivial for gradient flow, since $g_{GD}^{-1}(\theta) = 1$. For $m \odot w$, Jacobs & Burkholz (2025) have derived $g_{m \odot w}^{-1}(\theta) = \sqrt{\theta^2 + \gamma^2}$, where γ depends on the initialization scale and can change due to noise and regularization. In contrast, the inverse metric of HAM is not changed by these factors. To give an overview, the inverse metrics are also reported in Table 2.

The vanishing inverse metric problem For small γ and small weights θ , the inverse metric $\sqrt{\theta^2 + \gamma^2}$ of $m \odot w$ can get much smaller than 1 (see Figure 1). This implies that learning close to 0 is slowed down, which makes transitions through 0 (and sign flips of θ) much harder, slowing down convergence.

Table 2: Inverse metrics of gradient descent, the overparameterization $m \odot w$, and HAM.

	GD	$m \odot w$	HAM
$g^{-1}(\theta)$	1	$\sqrt{\theta^2 + \gamma^2}$	$1 + \alpha \theta $

Theorem 4.1 *If f is L -smooth (Definition A.1), satisfies the PL-inequality (A.2) or is convex and $\arg \min\{f(\theta) : \theta \in \mathbb{R}^n\}$ is non-empty, then the iterates θ_t converge to a minimizer of f for both metrics g_{GD} and $g_{m \odot w}$. Under the PL-inequality, the linear convergence rates are respectively Λ and $\Lambda \min_i \gamma_i$, where $\Lambda > 0$ is the PL-inequality constant.*

Proof. We can apply Theorem A.3 in Jacobs & Burkholz (2025) (Thm. A.7 in the appendix) and Theorem 4.14 in Li et al. (2022) (Thm. A.6 in the appendix). For the convergences rates it is sufficient to bound the inverse metrics from below such that we have $g_{GD} \geq 1$ and $g_{m \odot w} \geq \min_i \gamma_i$. \square

Riemannian gradient flow of HAM In comparison, HAM speeds up learning around 0. To show this and characterize HAM’s dynamics, we derive its gradient flow from Eqs. (GD;HYP) by writing out the iterates in sum notation and taking the learning rate $\eta \rightarrow 0$.

Theorem 4.2 *The Riemannian gradient flow ($\eta \rightarrow 0$) of Eqs. (GD;HYP) is:*

$$d\boldsymbol{\theta}_t = -(1 + \alpha|\boldsymbol{\theta}_t|) \odot \nabla f(\boldsymbol{\theta}_t) dt - \beta \boldsymbol{\theta}_t dt, \quad \boldsymbol{\theta}_0 = \boldsymbol{\theta}_{init}, \quad (4)$$

where $|\cdot|$ is applied pointwise. Moreover, if $\beta = 0$, the inverse metric is $g_{\text{HAM}}^{-1}(\boldsymbol{\theta}) = 1 + \alpha|\boldsymbol{\theta}|$.

Proof. This follows from writing out the sum update and then taking the limit to get an integral equation. The gradient flow then follows from the Leibniz rule. See Theorem B.3 in the appendix. \square

Convergence of HAM We analyze the inverse metric and convergence behavior of HAM when $\beta = 0$. In this case, the inverse metric is given by $g_{\text{HAM}}(\boldsymbol{\theta}) = 1 + \alpha|\boldsymbol{\theta}|$ (Table 2), indicating that HAM can converge faster than gradient descent depending on α and the magnitude of the weights. This stands in stark contrast with sparsification methods, where a decaying $\gamma \ll 1$ slows down movement. We formalize this behavior under the same conditions as Theorem 4.1:

Theorem 4.3 *Under the same setting as Theorem 4.1, the iterates of HAM in Eq. (GD,HYP) with $\beta = 0$, $\boldsymbol{\theta}_t$, converge to a minimizer of f . Moreover, the linear convergence rate is Λ under the PL-inequality.*

Proof. Similar as in Theorem 4.1 we again can lower bound $g_{\text{HAM}}^{-1} \geq 1$ for the convergence rate.

This proves that HAM avoids the vanishing inverse metric problem from the pointwise overparameterization $\boldsymbol{m} \odot \boldsymbol{w}$, while keeping the geometric benefits as we will see next. Furthermore, we discuss the case for $\beta > 0$ in §B.1.

Implicit bias of HAM We characterize the implicit bias of HAM by analyzing its associated Riemannian gradient flow. This confirms that HAM not only speeds up convergence with respect to $\boldsymbol{m} \odot \boldsymbol{w}$ and small γ , but also influences the nature of the solution. To show this, we compute the Bregman function R_α (see Definition A.4) such that its Hessian yields the required metric, i.e., $g_{\text{HAM}} = \nabla^2 R_\alpha$.

Lemma 4.4 *The function R_α for $\alpha \in \mathbb{R}$ is given by*

$$R_\alpha(\boldsymbol{\theta}) = \sum_i \frac{(\alpha|\theta_i| + 1) \ln(\alpha|\theta_i| + 1) - \alpha|\theta_i|}{\alpha^2} - \theta_i \frac{\text{sign}(\theta_{i,0})}{\alpha} \log(1 + \alpha|\theta_{i,0}|).$$

If $\alpha > 0$, R_α is a Bregman function (Definition A.4).

Proof. See Lemma B.4 in the appendix. \square

Concretely, we can use Lemma 4.4 to characterize the implicit bias for under-determined linear regression. Let $\{(z_i, y_i)\}_{i=1}^d \subset \mathbb{R}^n \times \mathbb{R}$ be a dataset of size d . The output of a linear model $\boldsymbol{\theta}$ on the i -th data is $z_i^T \boldsymbol{\theta}$. The goal therefore is to solve the regression for the target vector $\boldsymbol{y} = (y_1, y_2, \dots, y_d)^T$ and input vector $\boldsymbol{Z} = (z_1, z_2, \dots, z_d)$.

Theorem 4.5 *Consider the same setting as Theorem 4.3 with $\beta = 0$. Then, if $f(\boldsymbol{\theta}) := f(\boldsymbol{Z}^T \boldsymbol{\theta} - \boldsymbol{y})$, the gradient flow of $\boldsymbol{\theta}_t$ in Eq. (4) converges to the solution of the optimization problem: $\boldsymbol{\theta}_\infty = \arg \min_{\boldsymbol{Z}\boldsymbol{\theta}=\boldsymbol{y}} R_\alpha(\boldsymbol{\theta})$.*

Proof. Apply the mirror flow part of Theorem 4.17 (Li et al., 2022) for Bregman functions. \square

Theorem 4.5 provides an intuition about the type of solutions to which HAM converges. We are particularly interested in the shape of R_α when $\boldsymbol{\theta}_0 = \mathbf{0}$ (to understand sign flips). Note that the gradient flow is well defined at $\boldsymbol{\theta}_0$ if $\beta = 0$.

Theorem 4.6 *Let $\boldsymbol{\theta}_0 = \mathbf{0}$. Then, $R_\alpha \sim \|\boldsymbol{\theta}\|_{L_2}^2$ if $\alpha \rightarrow 0$, and $R_\alpha \sim \|\boldsymbol{\theta}\|_{L_1}$ if $\alpha \rightarrow \infty$, where \sim indicates proportionality, i.e., there exists some positive functions $h_1 : \mathbb{R} \rightarrow \mathbb{R}$ and $h_2 : \mathbb{R} \rightarrow \mathbb{R}$ in the neighborhood of the limiting point such that for all $\boldsymbol{\theta} \in \mathbb{R}^n$, $\lim_{\alpha \rightarrow 0} h_1(\alpha) R_\alpha(\boldsymbol{\theta}) = \|\boldsymbol{\theta}\|_{L_2}^2$ and $\lim_{\alpha \rightarrow \infty} h_2(\alpha) R_\alpha(\boldsymbol{\theta}) = \|\boldsymbol{\theta}\|_{L_1}$.*

Proof. See proof of Theorem B.5 in the appendix. \square

Theorem 4.6 is illustrated in Figure 2(b). R_α of HAM induces an implicit bias that interpolates between L_2 and L_1 , similarly to $\mathbf{m} \odot \mathbf{w}$ (Jacobs & Burkholz, 2025).

Remark 4.7 *In the $\alpha \rightarrow \infty$ setting, HAM induces an L_1 bias. However, in practice, due to discretizations, this setting would require a much smaller learning rate to ensure convergence. This makes HAM less suited to fully induce sparsity on its own than the related sparsification methods. Therefore, HAM is best used in combination with other methods to find sparse solutions, acting as a guide for sparse geometry during training.*

Remark 4.7 emphasizes that HAM needs a substantially large α to induce sparsity on its own. This is in line with our takeaway from §3: Our hyperbolic step primarily contributes to learning the correct magnitude of a weight and promotes sign flips. This differs from $\mathbf{m} \odot \mathbf{w}$ overparameterization, where sparsity emerges due to the inherently small inverse metric.

Remark 4.8 *In practice, we apply additional weight decay with strength $\beta > 0$. This promotes sparsity but does not change the inverse metric for HAM. In contrast, for $\mathbf{m} \odot \mathbf{w}$ it worsens the vanishing inverse metric problem (see Appendix F), as we learn from comparing gradient flows (Eq. 2 and Eq. 4). HAM has the advantage that we can freely tune α for the right amount of implicit sparsity. For details on how $\beta > 0$ influences Thms 4.3 and 4.5 see §B.1.*

5 EXPERIMENTS

Our main goal is to highlight the versatility of our novel optimizer step, HAM, and verify our theoretical insights into its mechanisms. To this end, we compare HAM to two algorithms that explicitly utilize the parameterization $\mathbf{m} \odot \mathbf{w}$: a) PiLoT (Jacobs & Burkholz, 2025), a continuous sparsification method, and b) Sign-In (Gadhikar et al., 2025), an optimization approach designed to improve training sparse masks (especially in the context of PaI). Sign-In promotes sign flips complementary to dense training by rescaling γ to 1 in intervals, partially mitigating the vanishing inverse metric problem but inducing frequent perturbations to the optimization (see Appendix F).

HAM, due to its implicit sparsity bias (Theorem 4.7) and improve plasticity, is particularly compatible with sparse training methods, as we showcase in multiple scenarios. We choose hyperparameters (α, β) based on a grid search for dense training (see Figure 11 and Figure 12). The chosen hyperparameters are transferred to all dense and sparse training methods. For ImageNet and Vision Transformers, we use $(\alpha, \beta) = (200, 1e - 3)$ and for CIFAR100 $(\alpha, \beta) = (200, 16e - 3)$.

HAM improves generalization in a way that is complementary to Sharpness Aware Minimization (SAM) (Foret et al., 2021). We also apply HAM to other tasks such as pre-training vision transformers, LLM fine-tuning and graph and node classification in Appendices G.3, G.6 and G.7. This demonstrates the general utility of HAM as an optimization principle. In addition, Appendix G.1 verifies the improved (sparse) implicit bias proven in Theorem 4.5 for underdetermined linear regression.

Dense training Table 3 demonstrates that HAM improves dense training for a ResNet50 on ImageNet (Deng et al., 2009). Moreover, HAM works complementary to Sharpness Aware Minimization (SAM) (Foret et al., 2021). Combining both algorithms (SAM-HAM) achieves the best overall performance. Table 3 further highlights that training HAM longer (using a similar compute budget as SAM, whose iterations are twice as expensive) achieves a similar improvement. Figure 10 tracks the total L_1 norm of the parameters during training to illustrate the complementary mechanisms of HAM and SAM. The same conclusions hold for similar experiments with the smaller vision benchmark CIFAR100 (Krizhevsky et al., 2009) (see Table 7). Furthermore, Table 8 showcases performance gains also for the transformer architecture DeiT (Touvron et al., 2021) trained on ImageNet with AdamW. A grid search for HAM’s hyperparameters α and β on ImageNet (Deng et al., 2009) and CIFAR100 (Krizhevsky et al., 2009) is visualized in Fig. 11 and 12. The best values for α are stable across different tasks, while β needs tuning similar to weight decay.

Sparsification We demonstrate that HAM improves state-of-the-art pruning methods AC/DC and RiGL, as well as random pruning at initialization with the same hyperparameter configuration used

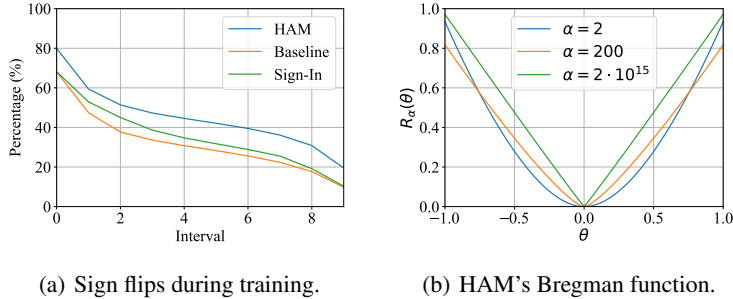


Figure 2: Demonstration of HAM’s mechanisms. (a) The percentage of sign flips during training for Random PaI with sparsity level 90% trained for 100 epochs, where each interval correspond to ten epochs. HAM is able to consistently perform more sign flips than both the baseline and Sign-In. (b) Plot of the normalized Bregman function R_α , where increasing α leads to an L_1 shape.

Table 3: HAM improves dense training of a ResNet50 on ImageNet.

	100 epochs	200 epochs	+ SAM, 100 epochs	+ SAM, 200 epochs
Baseline	76.72 ± 0.19	77.27 ± 0.13	77.10 ± 0.21	77.94 ± 0.16
HAM	77.51 ± 0.11	77.86 ± 0.05	77.92 ± 0.15	78.56 ± 0.12

in dense training. Table 4 illustrates that dense-to-sparse training becomes significantly better with HAM. Improvements are most significant for AC/DC, which uses dense training phases effectively. We attribute this also to the fact that AC/DC turns on parameters indiscriminately, while RiGL does so based on gradient information. The improvements over PILoT and Sign-In show that we successfully extract the main beneficial mechanism of the hyperbolic geometry while mitigating the downsides.

Sign flip mechanism We show that HAM outperforms Sign-In (Gadhikar et al., 2025), which promotes sign flips complementary to dense training and tries to mitigate the vanishing inverse metric problem by repeated parameter rescaling. HAM still induces more sign flips than Sign-In and standard training, as demonstrated by Figure 2(a), which is in line with our theory (see Appendix E). Supporting this, we show in Appendix G.4 the improvement for training with various fixed masks.

Table 4: Dense-to-sparse training and pruning at initialization with HAM on ImageNet with ResNet50.

Pruning type	Method	$s = 0.8$	$s = 0.9$	$s = 0.95$
PaI	Random	73.87(±0.06)	71.56(±0.03)	68.72(±0.05)
	Random + <i>Sign-In</i>	74.12(±0.09)	72.19(±0.18)	69.38(±0.1)
	Random + HAM	74.84(±0.09)	72.72(±0.03)	70.05(±0.06)
DtS	AC/DC	75.83(±0.02)	74.75(±0.02)	72.59(±0.11)
	AC/DC + <i>Sign-In</i>	75.9(±0.14)	74.74(±0.12)	72.88(±0.13)
	AC/DC + HAM	77.2(±0.14)	76.66(±0.12)	75.45(±0.13)
DST	RiGL	75.02(±0.1)	73.7(±0.2)	71.89(±0.07)
	RiGL + <i>Sign-In</i>	75.02(±0.1)	74.27(±0.08)	73.07(±0.17)
	RiGL + HAM	76.22(±0.07)	74.83(±0.08)	72.93(±0.1)
Cont. spars.	spread	72.64	71.84	69.47
	PILoT	75.62	74.73	71.3
	STR	75.49(±0.14)	72.4(±0.11)	64.94(±0.07)
	STR + HAM	76.37(±0.18)	75.01(±0.02)	71.41(±0.1)

6 CONCLUSION

We propose a new hyperbolic update step that can be combined with any first-order optimizer and that improves generalization of dense and sparse training, making it suitable as a general purpose optimizer. Our algorithm HAM (Hyperbolic Aware Minimization) mitigates the vanishing inverse metric of the pointwise overparameterization $m \odot w$ used in recent sparsification methods, while inducing a similar implicit bias. Due to discretization, it is more suitable to control the strength and shape of the bias—and accordingly improve generalization in general, especially for dense-to-sparse training. The main mechanisms how HAM achieves this are an implicit bias towards sparsity and an acceleration of learning that promotes parameter sign flips. It remains an interesting open question if different mirror maps could create better task and optimizer-specific awareness. For example, for some tasks one might want to take into account robustness; for the optimizer, it might be the momentum or normalization. This could lead to more algorithmic advances to improve generalization via implicit bias control and to new theory for understanding the success of deep learning algorithms. In particular, optimizers with implicit biases that emulate the positive effects of other types of overparameterization, without explicitly requiring huge models, may represent an important leap in reducing the high computational costs associated with deep learning.

ACKNOWLEDGEMENTS

The authors gratefully acknowledge the Gauss Centre for Supercomputing e.V. for funding this project by providing computing time on the GCS Supercomputer JUWELS at Jülich Supercomputing Centre (JSC). We also gratefully acknowledge funding from the European Research Council (ERC) under the Horizon Europe Framework Programme (HORIZON) for proposal number 101116395 SPARSE-ML.

REPRODUCIBILITY STATEMENT

For the theory, detailed proofs have been provided for the main statements in Appendix B and used previously known statements have been provided in Appendix A. For the experiments, the details are provided in Appendix G with each experiment having its own subsection with accompanied specifics. The code use for the experiments is also attached.

LLM STATEMENT

To improve fluency of the text sentence level editing has been done using large language models.

REFERENCES

- Felipe Alvarez, Jérôme Bolte, and Olivier Brahic. Hessian riemannian gradient flows in convex programming. *SIAM Journal on Control and Optimization*, 43(2):477–501, January 2004. ISSN 1095-7138. doi: 10.1137/s0363012902419977. URL <http://dx.doi.org/10.1137/s0363012902419977>.
- Shun-ichi Amari. Natural gradient works efficiently in learning. In *Unsupervised Learning: Foundations of Neural Computation*. The MIT Press, 05 1999. ISBN 9780262288033. doi: 10.7551/mitpress/7011.003.0010. URL <https://doi.org/10.7551/mitpress/7011.003.0010>.
- Amir Beck and Marc Teboulle. Mirror descent and nonlinear projected subgradient methods for convex optimization. *Operations Research Letters*, 31(3):167–175, 2003. ISSN 0167-6377. doi: [https://doi.org/10.1016/S0167-6377\(02\)00231-6](https://doi.org/10.1016/S0167-6377(02)00231-6). URL <https://www.sciencedirect.com/science/article/pii/S0167637702002316>.
- Jeremy Bernstein, Jiawei Zhao, Markus Meister, Ming-Yu Liu, Anima Anandkumar, and Yisong Yue. Learning compositional functions via multiplicative weight updates. In

- H. Larochelle, M. Ranzato, R. Hadsell, M.F. Balcan, and H. Lin (eds.), *Advances in Neural Information Processing Systems*, volume 33, pp. 13319–13330. Curran Associates, Inc., 2020. URL https://proceedings.neurips.cc/paper_files/paper/2020/file/9a32ef65c42085537062753ec435750f-Paper.pdf.
- Stephen P. Boyd and Lieven Vandenbergh. Convex optimization. 2009. URL <https://web.stanford.edu/~boyd/cvxbook/>.
- Stephen P. Boyd, Neal Parikh, Eric Chu, Borja Peleato, and Jonathan Eckstein. Distributed optimization and statistical learning via the alternating direction method of multipliers. *Found. Trends Mach. Learn.*, 3:1–122, 2011. URL <https://api.semanticscholar.org/CorpusID:51789432>.
- Shaked Brody, Uri Alon, and Eran Yahav. How attentive are graph attention networks? In *International Conference on Learning Representations*, 2022. URL <https://openreview.net/forum?id=F72ximsx7C1>.
- Tianlong Chen, Yu Cheng, Zhe Gan, Lu Yuan, Lei Zhang, and Zhangyang Wang. Chasing sparsity in vision transformers: An end-to-end exploration. *Advances in Neural Information Processing Systems*, 34:19974–19988, 2021.
- A. Cichocki, R. Zdunek, A.H. Phan, and S. Amari. *Nonnegative Matrix and Tensor Factorizations: Applications to Exploratory Multi-way Data Analysis and Blind Source Separation*. Wiley, 2009. ISBN 9780470747285. URL <https://books.google.de/books?id=KaxssMiWgswC>.
- J. Deng, W. Dong, R. Socher, L.-J. Li, K. Li, and L. Fei-Fei. ImageNet: A Large-Scale Hierarchical Image Database. In *CVPR09*, 2009.
- Utku Evci, Trevor Gale, Jacob Menick, Pablo Samuel Castro, and Erich Elsen. Rigging the lottery: Making all tickets winners. In *International Conference on Machine Learning*, pp. 2943–2952. PMLR, 2020.
- Mathieu Even, Scott Pehme, Suriya Gunasekar, and Nicolas Flammarion. (s)gd over diagonal linear networks: Implicit bias, large stepsizes and edge of stability. In A. Oh, T. Naumann, A. Globerson, K. Saenko, M. Hardt, and S. Levine (eds.), *Advances in Neural Information Processing Systems*, volume 36, pp. 29406–29448. Curran Associates, Inc., 2023. URL https://proceedings.neurips.cc/paper_files/paper/2023/file/5da6ce80e97671b70c01a2e703b868b3-Paper-Conference.pdf.
- Pierre Foret, Ariel Kleiner, Hossein Mobahi, and Behnam Neyshabur. Sharpness-aware minimization for efficiently improving generalization. In *International Conference on Learning Representations*, 2021. URL <https://openreview.net/forum?id=6Tm1mposlrM>.
- Jonathan Frankle and Michael Carbin. The lottery ticket hypothesis: Finding sparse, trainable neural networks. *arXiv: Learning*, 2018. URL <https://api.semanticscholar.org/CorpusID:53388625>.
- Jonathan Frankle and Michael Carbin. The lottery ticket hypothesis: Finding sparse, trainable neural networks. In *International Conference on Learning Representations*, 2019.
- Advait Gadhikar and Rebekka Burkholz. Masks, signs, and learning rate rewinding. In *Twelfth International Conference on Learning Representations*, 2024a. URL <https://openreview.net/forum?id=qODvxQ8TXW>.
- Advait Gadhikar, Tom Jacobs, Chao Zhou, and Rebekka Burkholz. Sign-in to the lottery: Reparameterizing sparse training. In *The Thirty-ninth Annual Conference on Neural Information Processing Systems*, 2025. URL <https://openreview.net/forum?id=iwKT7MEZZw>.
- Advait Harshal Gadhikar and Rebekka Burkholz. Masks, signs, and learning rate rewinding. In *International Conference on Learning Representations*, 2024b.
- Advait Harshal Gadhikar, Sohom Mukherjee, and Rebekka Burkholz. Why random pruning is all we need to start sparse. In *International Conference on Machine Learning*, 2023.

- Egor Gladin, Pavel Dvurechensky, Alexander Mielke, and Jia-Jie Zhu. Interaction-force transport gradient flows. *ArXiv*, abs/2405.17075, 2024. URL <https://api.semanticscholar.org/CorpusID:270063137>.
- Aaron Grattafiori, Abhimanyu Dubey, Abhinav Jauhri, Abhinav Pandey, Abhishek Kadian, Ahmad Al-Dahle, Aiesha Letman, Akhil Mathur, Alan Schelten, Alex Vaughan, et al. The llama 3 herd of models. *arXiv preprint arXiv:2407.21783*, 2024.
- Suriya Gunasekar, Blake Woodworth, Srinadh Bhojanapalli, Behnam Neyshabur, and Nathan Srebro. Implicit regularization in matrix factorization, 2017a. URL <https://arxiv.org/abs/1705.09280>.
- Suriya Gunasekar, Blake E Woodworth, Srinadh Bhojanapalli, Behnam Neyshabur, and Nati Srebro. Implicit regularization in matrix factorization. In I. Guyon, U. Von Luxburg, S. Bengio, H. Wallach, R. Fergus, S. Vishwanathan, and R. Garnett (eds.), *Advances in Neural Information Processing Systems*, volume 30. Curran Associates, Inc., 2017b. URL https://proceedings.neurips.cc/paper_files/paper/2017/file/58191d2a914c6dae66371c9dc91b41-Paper.pdf.
- Suriya Gunasekar, Jason Lee, Daniel Soudry, and Nathan Srebro. Characterizing implicit bias in terms of optimization geometry. In Jennifer Dy and Andreas Krause (eds.), *Proceedings of the 35th International Conference on Machine Learning*, volume 80 of *Proceedings of Machine Learning Research*, pp. 1832–1841. PMLR, 10–15 Jul 2018. URL <https://proceedings.mlr.press/v80/gunasekar18a.html>.
- Will Hamilton, Zhitao Ying, and Jure Leskovec. Inductive representation learning on large graphs. In I. Guyon, U. Von Luxburg, S. Bengio, H. Wallach, R. Fergus, S. Vishwanathan, and R. Garnett (eds.), *Advances in Neural Information Processing Systems*, volume 30. Curran Associates, Inc., 2017. URL https://proceedings.neurips.cc/paper_files/paper/2017/file/5dd9db5e033da9c6fb5ba83c7a7e9bea9-Paper.pdf.
- Song Han, Jeff Pool, John Tran, and William Dally. Learning both weights and connections for efficient neural network. *Advances in neural information processing systems*, 28, 2015.
- Jordan Hoffmann, Sebastian Borgeaud, Arthur Mensch, Elena Buchatskaya, Trevor Cai, Eliza Rutherford, Diego de Las Casas, Lisa Anne Hendricks, Johannes Welbl, Aidan Clark, et al. Training compute-optimal large language models. *arXiv preprint arXiv:2203.15556*, 2022.
- Weihua Hu, Matthias Fey, Marinka Zitnik, Yuxiao Dong, Hongyu Ren, Bowen Liu, Michele Catasta, and Jure Leskovec. Open graph benchmark: datasets for machine learning on graphs. In *Proceedings of the 34th International Conference on Neural Information Processing Systems, NIPS '20*, Red Hook, NY, USA, 2020. Curran Associates Inc. ISBN 9781713829546.
- Zhiqiang Hu, Yihuai Lan, Lei Wang, Wanyu Xu, Ee-Peng Lim, Roy Ka-Wei Lee, Lidong Bing, and Soujanya Poria. Llm-adapters: An adapter family for parameter-efficient fine-tuning of large language models. *arXiv preprint arXiv:2304.01933*, 2023.
- Tom Jacobs and Rebekka Burkholz. Mask in the mirror: Implicit sparsification. In *The Thirteenth International Conference on Learning Representations*, 2025. URL <https://openreview.net/forum?id=U47ymTS3ut>.
- Tom Jacobs, Chao Zhou, and Rebekka Burkholz. Mirror, mirror of the flow: How does regularization shape implicit bias? In *Forty-second International Conference on Machine Learning*, 2025. URL <https://openreview.net/forum?id=MLiR9LS5PW>.
- Adarsh Jamadandi, Celia Rubio-Madrigal, and Rebekka Burkholz. Spectral graph pruning against over-squashing and over-smoothing. In *The Thirty-eighth Annual Conference on Neural Information Processing Systems*, 2024. URL <https://openreview.net/forum?id=EMkrwJY2de>.
- Tian Jin, Michael Carbin, Dan Roy, Jonathan Frankle, and Gintare Karolina Dziugaite. Pruning’s effect on generalization through the lens of training and regularization. *Advances in Neural Information Processing Systems*, 35:37947–37961, 2022.

- Jared Kaplan, Sam McCandlish, Tom Henighan, Tom B Brown, Benjamin Chess, Rewon Child, Scott Gray, Alec Radford, Jeffrey Wu, and Dario Amodei. Scaling laws for neural language models. *arXiv preprint arXiv:2001.08361*, 2020.
- Mohammad Emtiyaz Khan and H. Rue. The bayesian learning rule. *J. Mach. Learn. Res.*, 24:281:1–281:46, 2021. URL <https://api.semanticscholar.org/CorpusID:235790670>.
- Thomas N. Kipf and Max Welling. Semi-supervised classification with graph convolutional networks. In *International Conference on Learning Representations*, 2017. URL <https://openreview.net/forum?id=SJU4ayYgl>.
- Jyrki Kivinen and Manfred Warmuth. Exponentiated gradient versus gradient descent for linear predictors. Technical report, USA, 1994.
- Chris Kolb, Tobias Weber, Bernd Bischl, and David Rügamer. Deep weight factorization: Sparse learning through the lens of artificial symmetries. In *The Thirteenth International Conference on Learning Representations*, 2025. URL <https://openreview.net/forum?id=vNd0Hr7mn5>.
- Alex Krizhevsky, Geoffrey Hinton, et al. Learning multiple layers of features from tiny images. 2009.
- Aditya Kusupati, Vivek Ramanujan, Raghav Somani, Mitchell Wortsman, Prateek Jain, Sham Kakade, and Ali Farhadi. Soft threshold weight reparameterization for learnable sparsity. In *Proceedings of the International Conference on Machine Learning*, July 2020.
- Denis Kuznedelev, Eldar Kurtic, Eugenia Iofinova, Elias Frantar, Alexandra Peste, and Dan Alistarh. Accurate neural network pruning requires rethinking sparse optimization. *Trans. Mach. Learn. Res.*, 2024, 2023. URL <https://api.semanticscholar.org/CorpusID:260611140>.
- Denis Kuznedelev, Eldar Kurtić, Elias Frantar, and Dan Alistarh. Cap: Correlation-aware pruning for highly-accurate sparse vision models. 36, 2024.
- Eren Mehmet Kiral, Thomas Möllenhoff, and Mohammad Emtiyaz Khan. The lie-group bayesian learning rule. In *International Conference on Artificial Intelligence and Statistics*, 2023. URL <https://api.semanticscholar.org/CorpusID:257404948>.
- Mike Lasby, Anna Golubeva, Utku Evci, Mihai Nica, and Yani Ioannou. Dynamic sparse training with structured sparsity. *arXiv preprint arXiv:2305.02299*, 2023.
- Namhoon Lee, Thalaisyasingam Ajanthan, and Philip H. S. Torr. Snip: single-shot network pruning based on connection sensitivity. In *International Conference on Learning Representations*, 2019.
- Hao Li, Asim Kadav, Igor Durdanovic, Hanan Samet, and Hans Peter Graf. Pruning filters for efficient convnets. In *International Conference on Learning Representations*, 2017.
- Zhiyuan Li, Tianhao Wang, Jason D. Lee, and Sanjeev Arora. Implicit bias of gradient descent on reparametrized models: On equivalence to mirror descent. In Alice H. Oh, Alekh Agarwal, Danielle Belgrave, and Kyunghyun Cho (eds.), *Advances in Neural Information Processing Systems*, 2022. URL https://openreview.net/forum?id=k4KHXS6_zOV.
- Shih-Yang Liu, Chien-Yi Wang, Hongxu Yin, Pavlo Molchanov, Yu-Chiang Frank Wang, Kwang-Ting Cheng, and Min-Hung Chen. Dora: Weight-decomposed low-rank adaptation. In *Forty-first International Conference on Machine Learning*, 2024.
- Shiwei Liu, Tianlong Chen, Xiaohan Chen, Li Shen, Decebal Constantin Mocanu, Zhangyang Wang, and Mykola Pechenizkiy. The unreasonable effectiveness of random pruning: Return of the most naive baseline for sparse training. In *International Conference on Learning Representations*, 2021a.
- Shiwei Liu, Lu Yin, Decebal Constantin Mocanu, and Mykola Pechenizkiy. Do we actually need dense over-parameterization? in-time over-parameterization in sparse training. In Marina Meila and Tong Zhang (eds.), *Proceedings of the 38th International Conference on Machine Learning*, volume 139 of *Proceedings of Machine Learning Research*, pp. 6989–7000. PMLR, 18–24 Jul 2021b.

- Yuankai Luo, Lei Shi, and Xiao-Ming Wu. Classic GNNs are strong baselines: Reassessing GNNs for node classification. In *The Thirty-eight Conference on Neural Information Processing Systems Datasets and Benchmarks Track*, 2024. URL <https://openreview.net/forum?id=xkljKdGe4E>.
- Yuankai Luo, Lei Shi, and Xiao-Ming Wu. GNN+: Can classic GNNs be strong baselines for graph-level tasks? In *International Conference on Machine Learning (ICML)*, 2025. URL <https://arxiv.org/abs/2502.09263>.
- Alexander Ly, Maarten Marsman, Josine Verhagen, Raoul Grasman, and Eric-Jan Wagenmakers. A tutorial on fisher information, 2017. URL <https://arxiv.org/abs/1705.01064>.
- Bochen Lyu and Zhanxing Zhu. Implicit bias of (stochastic) gradient descent for rank-1 linear neural network. In *Thirty-seventh Conference on Neural Information Processing Systems*, 2023. URL <https://openreview.net/forum?id=PjBEUTVzoe>.
- Negin Majidi, Ehsan Amid, Hossein Talebi, and Manfred K. Warmuth. Exponentiated gradient reweighting for robust training under label noise and beyond. *ArXiv*, abs/2104.01493, 2021. URL <https://api.semanticscholar.org/CorpusID:233024829>.
- James Martens. New insights and perspectives on the natural gradient method. *J. Mach. Learn. Res.*, 21:146:1–146:76, 2014. URL <https://api.semanticscholar.org/CorpusID:10284405>.
- Geoffrey J. McLachlan and Thiriyambakam Krishnan. The em algorithm and extensions. 1996. URL <https://api.semanticscholar.org/CorpusID:122530182>.
- Péter Mernyei and Cătălina Cangea. Wiki-cs: A wikipedia-based benchmark for graph neural networks, 2022. URL <https://arxiv.org/abs/2007.02901>.
- Alexander Mielke and Jia-Jie Zhu. Hellinger-kantorovich gradient flows: Global exponential decay of entropy functionals. 2025. URL <https://api.semanticscholar.org/CorpusID:275932494>.
- Decebal Constantin Mocanu, Elena Mocanu, Peter Stone, Phuong H. Nguyen, Madeleine Gibescu, and Antonio Liotta. Scalable training of artificial neural networks with adaptive sparse connectivity inspired by network science. *Nature Communications*, 9(1), jun 2018. doi: 10.1038/s41467-018-04316-3. URL <https://doi.org/10.1038/s41467-018-04316-3>.
- Sree Harsha Nelaturu, Advait Gadhikar, and Rebekka Burkholz. TurboPrune: High-Speed Distributed Lottery Ticket Training. URL <https://github.com/nelaturuharsha/TurboPrune>.
- Neal Parikh and Stephen Boyd. Proximal algorithms. *Found. Trends Optim.*, 1(3):127–239, January 2014. ISSN 2167-3888. doi: 10.1561/24000000003. URL <https://doi.org/10.1561/24000000003>.
- Shreyas Malakarjun Patil and Constantine Dovrolis. Phew: Constructing sparse networks that learn fast and generalize well without training data. In *International Conference on Machine Learning*, pp. 8432–8442. PMLR, 2021.
- Scott Pesme, Loucas Pillaud-Vivien, and Nicolas Flammarion. Implicit bias of SGD for diagonal linear networks: a provable benefit of stochasticity. In A. Beygelzimer, Y. Dauphin, P. Liang, and J. Wortman Vaughan (eds.), *Advances in Neural Information Processing Systems*, 2021. URL <https://openreview.net/forum?id=vvi7KqHQiA>.
- Alexandra Peste, Eugenia Iofinova, Adrian Vladu, and Dan Alistarh. Ac/dc: Alternating compressed/decompressed training of deep neural networks, 2021.
- Hoang Pham, The-Anh Ta, Shiwei Liu, Lichuan Xiang, Dung D. Le, Hongkai Wen, and Long Tran-Thanh. Towards data-agnostic pruning at initialization: What makes a good sparse mask? In *Thirty-seventh Conference on Neural Information Processing Systems*, 2023. URL <https://openreview.net/forum?id=xdOoCWCYaY>.

- Oleg Platonov, Denis Kuznedelev, Michael Diskin, Artem Babenko, and Liudmila Prokhorenkova. A critical look at the evaluation of GNNs under heterophily: Are we really making progress? In *The Eleventh International Conference on Learning Representations*, 2023. URL <https://openreview.net/forum?id=tJbbQfw-5wv>.
- Chendi Qian, Andrei Manolache, Kareem Ahmed, Zhe Zeng, Guy Van den Broeck, Mathias Niepert, and Christopher Morris. Probabilistically rewired message-passing neural networks. In *The Twelfth International Conference on Learning Representations*, 2024. URL <https://openreview.net/forum?id=Tj6Wcx7gVk>.
- Alex Renda, Jonathan Frankle, and Michael Carbin. Comparing rewinding and fine-tuning in neural network pruning. In *International Conference on Learning Representations*, 2020.
- Tyrrel R Rockafellar and Werner Fenchel. *Convex Analysis*. 1970. URL <https://api.semanticscholar.org/CorpusID:198120397>.
- Grant M. Rotskoff, Samy Jelassi, Joan Bruna, and Eric Vanden-Eijnden. Global convergence of neuron birth-death dynamics. *ArXiv*, abs/1902.01843, 2019. URL <https://api.semanticscholar.org/CorpusID:59604449>.
- Celia Rubio-Madrigal, Adarsh Jamadandi, and Rebekka Burkholz. GNNs getting comfy: Community and feature similarity guided rewiring. In *The Thirteenth International Conference on Learning Representations*, 2025. URL <https://openreview.net/forum?id=g6v09VxgFw>.
- Pedro Savarese, Hugo Silva, and Michael Maire. Winning the lottery with continuous sparsification, 2021.
- Oleksandr Shchur, Maximilian Mumme, Aleksandar Bojchevski, and Stephan Günnemann. Pitfalls of graph neural network evaluation, 2019. URL <https://arxiv.org/abs/1811.05868>.
- Yuesong Shen, Nico Daheim, Bai Cong, Peter Nickl, Gian Maria Marconi, Clement Bazan, Rio Yokota, Iryna Gurevych, Daniel Cremers, Mohammad Emtiyaz Khan, and Thomas Möllenhoff. Variational learning is effective for large deep networks. In *International Conference on Machine Learning (ICML)*, 2024. URL <https://arxiv.org/abs/2402.17641>.
- Sidak Pal Singh and Dan Alistarh. Woodfisher: Efficient second-order approximation for neural network compression. *Advances in Neural Information Processing Systems*, 33:18098–18109, 2020.
- Haoyuan Sun, Kwangjun Ahn, Christos Thrampoulidis, and Navid Azizan. Mirror descent maximizes generalized margin and can be implemented efficiently. In Alice H. Oh, Alekh Agarwal, Danielle Belgrave, and Kyunghyun Cho (eds.), *Advances in Neural Information Processing Systems*, 2022. URL <https://openreview.net/forum?id=0SV0leKNRAU>.
- Hidenori Tanaka, Daniel Kunin, Daniel L. Yamins, and Surya Ganguli. Pruning neural networks without any data by iteratively conserving synaptic flow. In *Advances in Neural Information Processing Systems*, 2020.
- Hugo Touvron, Matthieu Cord, Matthijs Douze, Francisco Massa, Alexandre Sablayrolles, and Hervé Jégou. Training data-efficient image transformers & distillation through attention. In *International conference on machine learning*, pp. 10347–10357. PMLR, 2021.
- Nisheeth K. Vishnoi. *Algorithms for Convex Optimization*. Cambridge University Press, 2021.
- Chaoqi Wang, Guodong Zhang, and Roger B. Grosse. Picking winning tickets before training by preserving gradient flow. In *International Conference on Learning Representations*, 2020.
- Blake Woodworth, Suriya Gunasekar, Jason D. Lee, Edward Moroshko, Pedro Savarese, Itay Golan, Daniel Soudry, and Nathan Srebro. Kernel and rich regimes in overparametrized models. In Jacob Abernethy and Shivani Agarwal (eds.), *Proceedings of Thirty Third Conference on Learning Theory*, volume 125 of *Proceedings of Machine Learning Research*, pp. 3635–3673. PMLR, 09–12 Jul 2020. URL <https://proceedings.mlr.press/v125/woodworth20a.html>.

Fan Wu and Patrick Rebeschini. Implicit regularization in matrix sensing via mirror descent. In *Neural Information Processing Systems*, 2021. URL <https://api.semanticscholar.org/CorpusID:235248126>.

Yuling Yan, Kaizheng Wang, and Philippe Rigollet. Learning gaussian mixtures using the wasserstein–fisher–rao gradient flow. *The Annals of Statistics*, 2024. URL <https://api.semanticscholar.org/CorpusID:273139387>.

Geng Yuan, Xiaolong Ma, Wei Niu, Zhengang Li, Zhenglun Kong, Ning Liu, Yifan Gong, Zheng Zhan, Chaoyang He, Qing Jin, et al. Mest: Accurate and fast memory-economic sparse training framework on the edge. *Advances in Neural Information Processing Systems*, 34:20838–20850, 2021.

Liu Ziyin and Zihao Wang. spread: Solving l1 penalty with sgd. In *International Conference on Machine Learning*, 2022. URL <https://api.semanticscholar.org/CorpusID:259075663>.

A OPTIMIZATION DEFINITIONS AND RESULTS

In this section we recall some basic definitions from convex and non-convex optimization.

Definition A.1 (*L-smooth*) A differentiable function $f : \mathbb{R}^n \rightarrow \mathbb{R}$ is said to be L -smooth if its gradient is Lipschitz continuous with constant $L > 0$. That is, for all $\boldsymbol{\theta}, \boldsymbol{\xi} \in \mathbb{R}^n$,

$$\|\nabla f(\boldsymbol{\theta}) - \nabla f(\boldsymbol{\xi})\| \leq L\|\boldsymbol{\theta} - \boldsymbol{\xi}\|,$$

or equivalently,

$$f(\boldsymbol{\xi}) \leq f(\boldsymbol{\theta}) + \langle \nabla f(\boldsymbol{\theta}), \boldsymbol{\xi} - \boldsymbol{\theta} \rangle + \frac{L}{2}\|\boldsymbol{\xi} - \boldsymbol{\theta}\|^2.$$

or equivalently,

$$\frac{1}{2}\|\nabla f(\boldsymbol{\theta})\|^2 \leq L(f(\boldsymbol{\theta}) - f^*),$$

where $f^* = \min_{\boldsymbol{\theta} \in \mathbb{R}^n} f(\boldsymbol{\theta})$.

Definition A.2 (*PL-inequality*) A differentiable function $f : \mathbb{R}^n \rightarrow \mathbb{R}$ satisfies the PL inequality with parameter $\Lambda > 0$ if for all $\boldsymbol{\theta} \in \mathbb{R}^n$,

$$\frac{1}{2}\|\nabla f(\boldsymbol{\theta})\|^2 \geq \Lambda(f(\boldsymbol{\theta}) - f^*),$$

where $f^* = \min_{\boldsymbol{\theta} \in \mathbb{R}^n} f(\boldsymbol{\theta})$.

Definition A.3 (*Legendre function Definition 3.8 (Li et al., 2022)*) Let $R : \mathbb{R}^d \rightarrow \mathbb{R} \cup \{\infty\}$ be a differentiable convex function. We say R is a Legendre function when the following holds:

- R is strictly convex on $\text{int}(\text{dom } R)$.
- For any sequence $\{\boldsymbol{\theta}_i\}_{i=1}^{\infty}$ going to the boundary of $\text{dom } R$, $\lim_{i \rightarrow \infty} \|\nabla R(\boldsymbol{\theta}_i)\|_{L_2}^2 = \infty$.

In order to recover the convergence result in Theorem 4.14 in (Li et al., 2022) the function R also needs to be a Bregman function, which we define in Definition A.4. First, let us denote with D_R denote the Bregman divergence with respect to the generator function R :

$$D_R(\boldsymbol{\theta}_1, \boldsymbol{\theta}_2) := R(\boldsymbol{\theta}_1) - R(\boldsymbol{\theta}_2) - \langle \nabla R(\boldsymbol{\theta}_2), \boldsymbol{\theta}_1 - \boldsymbol{\theta}_2 \rangle$$

for $\boldsymbol{\theta}_1, \boldsymbol{\theta}_2 \in \text{dom } R$.

Definition A.4 (*Bregman function Definition 4.1 (Alvarez et al., 2004)*) A function R is called a Bregman function if it satisfies the following properties:

- $\text{dom } R$ is closed. R is strictly convex and continuous on $\text{dom } R$. R is C^1 on $\text{int}(\text{dom } R)$.
- For any $\boldsymbol{\theta} \in \text{dom } R$ and $\gamma \in \mathbb{R}$, $\{\boldsymbol{\xi} \in \text{dom } R \mid D_R(\boldsymbol{\theta}, \boldsymbol{\xi}) \leq \gamma\}$ is bounded.
- For any $\boldsymbol{\theta} \in \text{dom } R$ and sequence $\{\boldsymbol{\theta}_i\}_{i=1}^{\infty} \subset \text{int}(\text{dom } R)$ such that $\lim_{i \rightarrow \infty} \boldsymbol{\theta}_i = \boldsymbol{\theta}$, it holds that $\lim_{i \rightarrow \infty} D_R(\boldsymbol{\theta}, \boldsymbol{\theta}_i) \rightarrow 0$.

Theorem A.5 (*Theorem 4.7 Alvarez et al. (2004)*) If R is a Legendre function with $\text{dom } R = \mathbb{R}^n$, then if the domain of the convex conjugate $\text{dom } R^* = \mathbb{R}^n$ implies that R is a Bregman function

From now on let R be a Bregman function A.4. Consider the Riemannian gradient flow:

$$d\boldsymbol{\theta}_t = -\nabla^2 R^{-1}(\boldsymbol{\theta}_t) \nabla f(\boldsymbol{\theta}_t) dt, \quad \boldsymbol{\theta}_0 = \boldsymbol{\theta}_{init}.$$

This covers all settings considered in the main text: gradient descent, $\mathbf{m} \odot \mathbf{w}$ and HAM as shown in Lemma B.4.

Theorem A.6 (*Theorem 4.14 (Li et al., 2022)*) Assume that R is a Bregman function and that f is quasi-convex, ∇f is locally Lipschitz and $\text{argmin}\{f(\boldsymbol{\theta}) \mid \boldsymbol{\theta} \in \mathbb{R}^n\}$ is non-empty. Then as $t \rightarrow \infty$, $\boldsymbol{\theta}_t$ converges to some critical point $\boldsymbol{\theta}^*$. Moreover, if f is convex $\boldsymbol{\theta}_t$ converges to a minimizer of f .

Theorem A.7 (Theorem A.3 (Jacobs & Burkholz, 2025)) Consider the same setting as Theorem A.6. Assume R satisfies for all $\theta \in \mathbb{R}^n$,

$$\mathbf{z}^T (\nabla^2 R(\theta))^{-1} \mathbf{z} \geq \sigma \|\mathbf{z}\|_{L_2}^2 \quad \forall \mathbf{z} \in \mathbb{R}^n. \quad (5)$$

Furthermore, assume f satisfies the PL-inequality (A.2). Then θ_t converges to a minimizer of f . Furthermore, the loss converges linearly with rate $\sigma\Lambda$.

B PROOFS OF THEORETICAL STATEMENTS

Here we provide detailed proofs of the main statements in the paper. The theorems correspondence is:

- The proof of Theorem 3.1 is in B.1.
- The proof of Theorem 4.2 is in B.3.
- The proof of Lemma 4.4 is in B.4.
- The proof of Theorem 4.6 is in B.5.

Theorem B.1 (Theorem 3.1) *If $\mathbf{m}_0 = \text{sign}(\boldsymbol{\theta}_0)\mathbf{w}_0 = \sqrt{|\boldsymbol{\theta}_0|}$, then*

$$\boldsymbol{\theta}_{k+1} = \boldsymbol{\theta}_k \exp(-\eta(2\text{sign}(\boldsymbol{\theta}_k)\nabla f(\boldsymbol{\theta}_k) + 4\beta)) \quad (6)$$

is equivalent to Eq. (1) up-to first order Taylor approximation.

First we use the Taylor approximation of the exponential function $\exp z \simeq 1 + z + \mathcal{O}(z^2)$ to get the update:

$$\boldsymbol{\theta}_{k+1} \simeq \boldsymbol{\theta}_k - 2\eta|\boldsymbol{\theta}_k|\nabla f(\boldsymbol{\theta}_k) - 4\eta\beta\boldsymbol{\theta}_k + \mathcal{O}(\eta^2).$$

We show this is equivalent up to first order to the gradient descent of the overparameterization:

$$\boldsymbol{\theta}_{k+1} = \mathbf{m}_{k+1} \odot \mathbf{w}_{k+1} \simeq \boldsymbol{\theta}_k - \eta(\mathbf{m}_k^2 + \mathbf{w}_k^2)\nabla f(\boldsymbol{\theta}_k) - 4\eta\beta\boldsymbol{\theta}_k.$$

To do so, we show that $\mathbf{m}_k^2 + \mathbf{w}_k^2 = 2|\boldsymbol{\theta}_k|$ for all $k \in [T]$ up to zeroth-order approximation by induction. For $k = 0$, the statement holds per assumption on the initialization. The induction step is:

$$\mathbf{m}_{k+1}^2 + \mathbf{w}_{k+1}^2 = \mathbf{m}_k^2 + \mathbf{w}_k^2 - 4\boldsymbol{\theta}_k\eta\nabla f(\boldsymbol{\theta}_k) - 4\eta\beta\boldsymbol{\theta}_k + \eta^2(\mathbf{m}_k^2 + \mathbf{w}_k^2)\nabla f(\boldsymbol{\theta}_k)^2 \simeq 2|\boldsymbol{\theta}_k| + \mathcal{O}(\eta).$$

This concludes the induction and the proof. \square

Corollary B.2 *Exponential gradient descent can not move through zero, preventing sign flips.*

Proof. The operation $\exp(\cdot)$ is always non-negative. Therefore multiplying with it will always keep the same sign since the sign operator is pointwise distributive:

$$\begin{aligned} \text{sign}(\boldsymbol{\theta}_{k+1}) &= \text{sign}(\boldsymbol{\theta}_k) \exp(-\eta(2\text{sign}(\boldsymbol{\theta}_k)\nabla f(\boldsymbol{\theta}_k) + 4\beta)) \\ &= \text{sign}(\boldsymbol{\theta}_k)\text{sign}(\exp(-\eta(2\text{sign}(\boldsymbol{\theta}_k)\nabla f(\boldsymbol{\theta}_k) + 4\beta))) \\ &= \text{sign}(\boldsymbol{\theta}_k). \end{aligned}$$

Note we use L -smoothness and sufficient small learning rate to ensure bounded gradient preventing $\nabla f(\boldsymbol{\theta}_k) \rightarrow \infty$. If the gradient explodes we still can only end up in zero leading to $\text{sign}(\boldsymbol{\theta}_{k+1}) = \mathbf{0}$ so also no sign flip in that case. \square

Theorem B.3 (Theorem 4.2) *The gradient flow ($\eta \rightarrow 0$) of Eqs. (GD;HYP) is given by:*

$$d\boldsymbol{\theta}_t = -\nabla f(\boldsymbol{\theta}_t)dt - |\boldsymbol{\theta}_t|(\alpha\nabla f(\boldsymbol{\theta}_t) + \text{sign}(\boldsymbol{\theta}_t)\beta)dt, \quad \boldsymbol{\theta}_0 = \boldsymbol{\theta}_{init}.$$

Writing out the computation of iterates $\boldsymbol{\theta}_k$ give us:

$$\boldsymbol{\theta}_k = \boldsymbol{\theta}_0 \exp\left(\sum_{j=0}^{k-1} -\eta\alpha\text{sign}(\boldsymbol{\theta}_j)\nabla f(\boldsymbol{\theta}_j) - \eta\beta\right) - \sum_{j=0}^{k-1} \eta\nabla f(\boldsymbol{\theta}_j) \exp\left(-\sum_{l=j}^{k-1} \eta\alpha\text{sign}(\boldsymbol{\theta}_l)\nabla f(\boldsymbol{\theta}_l) - \eta\beta\right).$$

This allows use to take $\eta \rightarrow 0$ and get an integral equation for the dynamics:

$$\boldsymbol{\theta}_t = \boldsymbol{\theta}_0 \exp\left(-\int_0^t \alpha\text{sign}(\boldsymbol{\theta}_s)\nabla f(\boldsymbol{\theta}_s) + \beta ds\right) - \int_0^t \nabla f(\boldsymbol{\theta}_s) \exp\left(-\int_s^t \alpha\text{sign}(\boldsymbol{\theta}_c)\nabla f(\boldsymbol{\theta}_c) + \beta dc\right) ds. \quad (7)$$

Differentiating the first term under the Leibniz rule gives:

$$\begin{aligned} & \frac{d}{dt} \boldsymbol{\theta}_0 \exp \left(- \int_0^t \alpha \operatorname{sign}(\boldsymbol{\theta}_s) \nabla f(\boldsymbol{\theta}_s) + \beta ds \right) = \\ & \boldsymbol{\theta}_0 \exp \left(- \int_0^t \alpha \operatorname{sign}(\boldsymbol{\theta}_s) \nabla f(\boldsymbol{\theta}_s) - \beta ds \right) (-\alpha \operatorname{sign}(\boldsymbol{\theta}_t) \nabla f(\boldsymbol{\theta}_t) + \beta) \end{aligned}$$

Next, differentiate the second term under the Leibniz rule:

$$\begin{aligned} & \frac{d}{dt} \left(- \int_0^t \nabla f(\boldsymbol{\theta}_s) \exp \left(- \int_s^t \alpha \operatorname{sign}(\boldsymbol{\theta}_c) \nabla f(\boldsymbol{\theta}_c) + \beta dc \right) ds \right) = \\ & -\nabla f(\boldsymbol{\theta}_t) - \int_0^t \frac{d}{dt} \nabla f(\boldsymbol{\theta}_s) \exp \left(- \int_s^t \alpha \operatorname{sign}(\boldsymbol{\theta}_c) \nabla f(\boldsymbol{\theta}_c) + \beta dc \right) ds = \\ & -\nabla f(\boldsymbol{\theta}_t) dt - \int_0^t \nabla f(\boldsymbol{\theta}_s) \exp \left(- \int_s^t \alpha \operatorname{sign}(\boldsymbol{\theta}_c) \nabla f(\boldsymbol{\theta}_c) + \beta dc \right) ds (-\alpha \operatorname{sign}(\boldsymbol{\theta}_t) \nabla f(\boldsymbol{\theta}_t) - \beta) \end{aligned}$$

Combining gives by noticing the form of $\boldsymbol{\theta}_t$:

$$\begin{aligned} d\boldsymbol{\theta}_t &= -\nabla f(\boldsymbol{\theta}_t) dt - \boldsymbol{\theta}_t (\alpha \operatorname{sign}(\boldsymbol{\theta}_t) \nabla f(\boldsymbol{\theta}_t) + \beta) dt \\ &= -\nabla f(\boldsymbol{\theta}_t) dt - |\boldsymbol{\theta}_t| (\alpha \nabla f(\boldsymbol{\theta}_t) + \operatorname{sign}(\boldsymbol{\theta}_t) \beta) dt \end{aligned}$$

□

Lemma B.4 (Lemma 4.4) *The Bregman function R_α for $\alpha > 0$ is given by:*

$$R_\alpha(\boldsymbol{\theta}) = \sum_i \frac{(\alpha |\theta_i| + 1) \ln(\alpha |\theta_i| + 1) - \alpha |\theta_i|}{\alpha^2} - \theta_i \frac{\operatorname{sign}(\theta_{i,0})}{\alpha} \log(1 + \alpha |\theta_{i,0}|)$$

Proof.

We first construct the mirror map R_α by using the corresponding Hessian g_{HAM} . Next we check that R_α is a Bregman function. The Hessian of the mirror map $R_\alpha(\boldsymbol{\theta})$ is:

$$\nabla^2 R_\alpha(\boldsymbol{\theta}) = \frac{1}{1 + \alpha |\boldsymbol{\theta}|}$$

Moreover we need $\nabla R_\alpha(\boldsymbol{\theta}_0) = 0$. Therefore by integrating twice, R_α for $\alpha > 0$ is given by:

$$R_\alpha(\boldsymbol{\theta}) = \sum_i \frac{(\alpha |\theta_i| + 1) \ln(\alpha |\theta_i| + 1) - \alpha |\theta_i|}{\alpha^2} - \theta_i \frac{\operatorname{sign}(\theta_{i,0})}{\alpha} \log(1 + \alpha |\theta_{i,0}|)$$

It remains to be checked if R_α is Bregman. For this we use a relationship between Legendre and Bregman functions. We first show that R_α is Legendre and its convex conjugate as well. Then it follows from Theorem A.5 that R_α is Bregman for $\alpha > 0$.

Note that we have $\operatorname{dom} R_\alpha = \operatorname{int}(\operatorname{dom} R_\alpha) = \mathbb{R}^n$. R_α is strictly convex as for all $\boldsymbol{\theta} \in \mathbb{R}^n$ the Hessian is positive definite. This shows the first statement. Next, since R_α is separable we can show the second statement for each parameter separately. Take a sequence $\{\theta_{i,j}\}_{i=1}^\infty$ for coordinate $j \in [n]$ such that $|\theta_{i,j}| \rightarrow \infty$ then by construction of R_α we have

$$\lim_{i \rightarrow \infty} \partial_j R_\alpha(\theta_{i,j})^2 = \infty$$

as $|\cdot|$ and $\log(\cdot)$ are increasing functions. Therefore R_α is Legendre.

The convex conjugate gradient $\operatorname{dom} \nabla R_\alpha^* = (\operatorname{range} \nabla R_\alpha)^{-1} = \mathbb{R}^n$. Therefore since $\mathbb{R}^n = \operatorname{dom} \nabla R_\alpha^* \subset \operatorname{dom} R_\alpha^*$ we can apply Theorem A.5. This concludes the result. □

Theorem B.5 (Theorem 4.6) *Let $\boldsymbol{\theta}_0 = \mathbf{0}$, then $R_\alpha \sim \|\boldsymbol{\theta}\|_{L_2}^2$ if $\alpha \rightarrow 0$ and $R_\alpha \sim \|\boldsymbol{\theta}\|_{L_1}$ if $\alpha \rightarrow \infty$, where \sim indicates proportionality i.e. there exists some positive functions $h_1 : \mathbb{R} \rightarrow \mathbb{R}$ and $h_2 : \mathbb{R} \rightarrow \mathbb{R}$ in the neighborhood of the limiting point such that for all $\boldsymbol{\theta} \in \mathbb{R}^n$, $\lim_{\alpha \rightarrow 0} h_1(\alpha) R_\alpha(\boldsymbol{\theta}) = \|\boldsymbol{\theta}\|_{L_2}^2$ and $\lim_{\alpha \rightarrow \infty} h_2(\alpha) R_\alpha(\boldsymbol{\theta}) = \|\boldsymbol{\theta}\|_{L_1}$.*

Proof. The first statement follows from the Taylor approximation:

$$R_\alpha \simeq \sum_i \theta_i^2 + \frac{1}{\alpha} |\theta_i| - \frac{1}{\alpha} |\theta_i| \simeq \|\boldsymbol{\theta}\|_{L_2}^2$$

which is valid if $|\theta_i| \ll \frac{1}{\alpha}$ so $h_1(\alpha) = 1$.

For large $\alpha > 0$ we have that $R_\alpha \simeq \sum_i \frac{|\theta_i|}{\alpha} \log(\alpha |\theta_i|)$. Therefore, we have

$$\frac{\alpha}{\log(\alpha)} R_\alpha(\boldsymbol{\theta}) \simeq \sum_i |\theta_i| = \|\boldsymbol{\theta}\|_{L_1},$$

so $h_2 = \frac{\alpha}{\log(\alpha)}$, which is positive $\alpha > 1$. This concludes the proof. \square

The proof of Theorem B.5 follows similar steps as that of Woodworth et al. (2020).

Sign discrepancy In our implemented HAM algorithm (HYP*) we use $\text{sign}(\boldsymbol{\theta}_{k+\frac{1}{2}})$ instead of $\text{sign}(\boldsymbol{\theta}_k)$ from the derived step (HYP). We now argue why this does not change the implications of our theory, as their gradient flows are equivalent. We show in Thm. B.6 that, in continuous time, the iterates (GD;HYP*) follow a jump process. For this jump process, the jump vanishes in the flow setting, leading to no discrepancy between using either version. In discrete time, however, this may not be the case. We provide an explanation for the effect in discrete time in Appendix D. The main implication of the flow being the same is that at the end of training the implicit bias is the same, as the end corresponds to smaller learning rates.

Theorem B.6 Initialize $\boldsymbol{\theta}_{init} \neq 0$. Then the gradient flow of HAM i.e. Eqs. (GD;HYP*) ($\eta \rightarrow 0$) is given by:

$$d\tilde{\boldsymbol{\theta}}_t = -\nabla f(\tilde{\boldsymbol{\theta}}_t) dt - |\tilde{\boldsymbol{\theta}}_t| \left(\alpha \nabla f(\tilde{\boldsymbol{\theta}}_t) + \text{sign}(\tilde{\boldsymbol{\theta}}_t) \beta \right) dt \quad \tilde{\boldsymbol{\theta}}_0 = \boldsymbol{\theta}_{init}. \quad (8)$$

Proof. The statement follows from making the observation: Sign flips can only occur near zero; further away the processes are equivalent.

Let $\tilde{\boldsymbol{\theta}}_t$ denote the resulting process with $\eta \rightarrow 0$ and $\boldsymbol{\theta}_t$ the signed gradient flow. $\tilde{\boldsymbol{\theta}}_t$ does not have to be gradient flow as it can have discontinuous jumps due to the sign inconsistency. We can write the update as follows:

$$\begin{aligned} \tilde{\boldsymbol{\theta}}_k &= \tilde{\boldsymbol{\theta}}_0 \exp \left(\sum_{j=0}^{k-1} -\eta \alpha \text{sign}(\tilde{\boldsymbol{\theta}}_j) \nabla f(\tilde{\boldsymbol{\theta}}_j) - \eta \beta - \eta \alpha \left(\text{sign}(\tilde{\boldsymbol{\theta}}_{j+\frac{1}{2}}) - \text{sign}(\tilde{\boldsymbol{\theta}}_j) \right) \nabla f(\tilde{\boldsymbol{\theta}}_j) \right) - \\ &\sum_{j=0}^{k-1} \eta \nabla f(\boldsymbol{\theta}_j) \exp \left(- \sum_{l=j}^{k-1} \eta \alpha \text{sign}(\boldsymbol{\theta}_l) \nabla f(\boldsymbol{\theta}_l) - \eta \beta - \eta \alpha \left(\text{sign}(\tilde{\boldsymbol{\theta}}_{j+\frac{1}{2}}) - \text{sign}(\tilde{\boldsymbol{\theta}}_j) \right) \nabla f(\tilde{\boldsymbol{\theta}}_j) \right). \end{aligned}$$

Then the discrepancy $\left(\text{sign}(\tilde{\boldsymbol{\theta}}_{j+\frac{1}{2}}) - \text{sign}(\tilde{\boldsymbol{\theta}}_j) \right)$ between the signs becomes a $\delta : \mathbb{R}^n \rightarrow \mathbb{R}^n$ function i.e.

$$\delta(\boldsymbol{\theta}) = \begin{cases} 0 & \text{if } \theta_i \neq 0 \\ 2 & \text{if } \theta_i = 0^+ \\ -2 & \text{if } \theta_i = 0^- \end{cases}, \quad \text{for } i \in [n]$$

The process for $\tilde{\boldsymbol{\theta}}_t$ with $\eta \rightarrow 0$ can be written as

$$\begin{aligned} \boldsymbol{\theta}_t &= \boldsymbol{\theta}_0 \exp \left(- \int_0^t \alpha \text{sign}(\boldsymbol{\theta}_s) \nabla f(\boldsymbol{\theta}_s) + \beta - \alpha \delta(\tilde{\boldsymbol{\theta}}_s) \nabla f(\tilde{\boldsymbol{\theta}}_s) ds \right) \\ &- \int_0^t \nabla f(\boldsymbol{\theta}_s) \exp \left(- \int_s^t \alpha \text{sign}(\boldsymbol{\theta}_c) \nabla f(\boldsymbol{\theta}_c) + \beta - \alpha \delta(\tilde{\boldsymbol{\theta}}_c) \nabla f(\tilde{\boldsymbol{\theta}}_c) dc \right) ds. \end{aligned}$$

Differentiating under the Leibniz rule gives:

$$d\tilde{\boldsymbol{\theta}}_t = -\nabla f(\tilde{\boldsymbol{\theta}}_t) dt - |\tilde{\boldsymbol{\theta}}_t| \left(\alpha \nabla f(\tilde{\boldsymbol{\theta}}_t) + \text{sign}(\tilde{\boldsymbol{\theta}}_t) \beta + \alpha \delta \nabla f(\tilde{\boldsymbol{\theta}}_t) \right) dt \quad \tilde{\boldsymbol{\theta}}_0 = \boldsymbol{\theta}_{init}.$$

where $\delta : \mathbb{R}^n \rightarrow \mathbb{R}^n$ is a delta function for every coordinate. Therefore, the jumps vanish as they are multiplied with $|\tilde{\theta}|$ we have that

$$d\tilde{\theta}_t = -\nabla f(\tilde{\theta}_t)dt - |\tilde{\theta}_t| \left(\alpha \nabla f(\tilde{\theta}_t) + \text{sign}(\tilde{\theta}_t) \beta \right) dt \quad \tilde{\theta}_0 = \tilde{\theta}_{init}.$$

which is equivalent to the gradient flow of Theorem B.3. \square

B.1 THE EFFECT OF NON-ZERO β

The convergence and implicit bias results Thms 4.3 and 4.5 focus on the case $\beta = 0$. In the follow, we discuss general the case of $\beta \geq 0$. First, the flow takes the general form:

$$d\theta_t = -g_t^{-1}(\theta_t) \nabla f(\theta_t) dt - \beta \theta_t dt, \quad \theta_0 = \theta_{init}. \quad (9)$$

We have for $m \odot w$ that $g_{t, m \odot w}^{-1}(\theta_t) = \sqrt{\theta_t^2 + \gamma_t^2}$ and for HAM we have $g_{HAM}^{-1}(\theta_t) = 1 + \alpha |\theta_t|$ in line with Table 2. For $\beta > 0$, we can define the on-manifold-regularization. This quantity determines the corresponding explicit regularization.

Definition B.7 For a time varying Riemannian gradient flow with off manifold weight decay Eq. (9), the on-manifold-regularization is given by

$$M_t(\theta) := \sum_{i \in [n]} \int^{\theta_i} g_{t,i}(z_i) z_i dz_i$$

where $g_{t,i}$ is the i -th component of the seperable metric tensor.

Using Definition B.7, we can compute M_t in both cases. This gives

$$M_{t, m \odot w}(\theta) = \sum_{i \in [n]} \sqrt{\theta_i^2 + \gamma_{t,i}^2} \text{ and } M_{HAM}(\theta) = \sum_{i \in [n]} \frac{\alpha |\theta_i| - \ln(|\alpha |\theta_i| + 1|)}{\alpha^2}. \quad (10)$$

Knowing this, we can adapt the convergence result. As both on-manifold-regularizations are convex, we converge to the minimizer of the objective function $f + \beta M$, assuming that there exists an M such that $M_t \rightarrow M$ for $t \rightarrow \infty$. Note that, for $m \odot w$, we have that $M_t \rightarrow \|\cdot\|_{L_1}$ for $t \rightarrow \infty$. This matches the LASSO optimization objective derived in spred (Ziyin & Wang, 2022). Additionally for HAM, we have that $\alpha M_{HAM} \rightarrow \|\cdot\|_{L_1}$ for $\alpha \rightarrow \infty$, indicating that we induce less sparsity, as we rescale with α . Concretely, for a fixed β and large α , we approximately solve the LASSO objective with regularization coefficient β/α . Note that for large α , the explicit regularization strength decays while the implicit regularization gets closer to L_1 .

Furthermore, to obtain the implicit bias result, we use the mirror flow formulation. We know from (Jacobs & Burkholz, 2025) that $m \odot w$ corresponds to a time-varying mirror flow for which we need $\beta \rightarrow 0$ to recover optimality. In contrast, for HAM we get the following mirror flow:

$$d\nabla R_\alpha(\theta_t) = - \left(\nabla f(\theta_t) + \beta \frac{\theta_t}{1 + \alpha |\theta_t|} \right) dt, \quad \theta_0 = \theta_{init}.$$

This follows from the new objective function $f + \beta M_{HAM}$. To fulfill the optimality condition in the implicit bias result for linear regression, we would need to show that the mirror flow is in the span of Z^T to satisfy the KKT condition. This can only be guaranteed when the regularization is turned off. Therefore, similarly to $m \odot w$, we would need to turn-off the regularization at the end of training to obtain optimality.

C FISHER INFORMATION DERIVATIONS

Our algorithm can be interpreted through the lens of natural gradient descent (Amari, 1999; Martens, 2014). Each optimizer step corresponds to a natural gradient update $\theta_{k+1} = \theta_k - \eta g^{-1}(\theta_k) \nabla f(\theta_k)$, with g is now the Fisher information. The key insight is that parameters follow a known parameterized distribution that is learned by the optimizer. For gradient descent, $g_{\text{GD}}(\theta) = \mathbf{1}$, which corresponds to a normally distributed random variable θ with unit variance and learnable mean; i.e., $\theta = \mathbb{E}[X]$. Thus we can interpret θ as the mean of a normal distribution whose *position* is learned.

In contrast, the hyperbolic step (HYP) on its own corresponds to $g_{\text{HYP}}(\theta) := 1/|\theta|$, which directly follows from the first order approximation of the exponential function. Similarly, we can match a random variables Fisher information to the metric $g_{\text{HYP}}(\theta)$. It corresponds to a random variable X parameterized as a normal distribution with unit variance: $\mathcal{N}(2\sqrt{|\theta|}, \mathbf{I})$. In this view, weights are recovered via $\theta = \frac{1}{4} \text{sign}(\theta) \mathbb{E}[X]^2$, by using $\mathbb{E}[X] = 2\sqrt{|\theta|}$. This means that we learn the *magnitude* of the expected position. Furthermore, if the sign is not correct, the hyperbolic step (HYP) will move the parameter exponentially fast towards zero, facilitating its sign flip. We provide derivations in next paragraph. To summarize, our combined update can be interpreted as follows:

Learn the position (GD), and then the magnitude if the sign is correct; else move fast to zero (HYP).

This mechanism is crucial to facilitate sparse training (Gadhikar & Burkholz, 2024a; Gadhikar et al., 2025), as portrayed in our experiments (§ 5), where HAM considerably boosts its performance.

Derivations of the Fisher information We provide here the Fisher information $\mathcal{I} := g$ calculations for one dimensional random variables $\mathcal{N}(\theta, 1)$ and $\mathcal{N}(\sqrt{|\theta|}, 1)$. The Fisher information is defined as see for example Definition 1.1 in (Ly et al., 2017):

$$\mathcal{I}(\theta) = \mathbb{E}_X \left[\left(\frac{\partial}{\partial \theta} \log f(X; \theta) \right)^2 \right] \quad (11)$$

where f is the probability density function of the random variable X and \mathbb{E} is the expectation with respect to the random variable.

Let $X \sim \mathcal{N}(\theta, 1)$, where $\theta \in \mathbb{R}$ is the mean parameter. The likelihood function is:

$$f(X; \theta) = \frac{1}{\sqrt{2\pi}} \exp\left(-\frac{1}{2}(X - \theta)^2\right)$$

Taking the natural logarithm:

$$\ell(\theta) = \log f(X; \theta) = -\frac{1}{2} \log(2\pi) - \frac{1}{2}(X - \theta)^2$$

The score function is:

$$\frac{d\ell}{d\theta} = (X - \theta)$$

Then the Fisher Information is given by:

$$\mathcal{I}_{\text{GD}}(\theta) = \mathbb{E} \left[\left(\frac{d\ell}{d\theta} \right)^2 \right] = \mathbb{E}[(X - \theta)^2] = \text{Var}(X) = 1$$

Let $X \sim \mathcal{N}(2\sqrt{|\theta|}, 1)$. The likelihood function is:

$$f(X; \theta) = \frac{1}{\sqrt{2\pi}} \exp\left(-\frac{1}{2}(X - 2\sqrt{|\theta|})^2\right)$$

The log-likelihood function is:

$$\ell(\theta) = -\frac{1}{2} \log(2\pi) - \frac{1}{2}(X - 2\sqrt{|\theta|})^2$$

Differentiate to get the score function:

$$\frac{d\ell}{d\theta} = (X - 2\sqrt{|\theta|}) \cdot \left(-\frac{\text{sign}(\theta)}{\sqrt{|\theta|}} \right) = -\text{sign}(\theta) \frac{X - 2\sqrt{\theta}}{\sqrt{\theta}}$$

Now square the score and take the expectation:

$$\mathcal{I}_{\text{HYP}}(\theta) = \mathbb{E} \left[\left(\frac{d\ell}{d\theta} \right)^2 \right] = \mathbb{E} \left[\left(\frac{X - 2\sqrt{|\theta|}}{\sqrt{|\theta|}} \right)^2 \right] = \frac{1}{|\theta|} \mathbb{E}[(X - 2\sqrt{|\theta|})^2] = \frac{1}{|\theta|} \text{Var}(X) = \frac{1}{|\theta|}$$

Note that instead of being part of the exponential family of distributions this distribution is part of the curved exponential family distributions.

D DIFFERENT SIGNS IN THE EXPONENTIAL UPDATE

In this section, we show that using the updated signs $\text{sign}(\boldsymbol{\theta}_{t+\frac{1}{2}})$ in the hyperbolic step (HYP) instead of the original ones $\text{sign}(\boldsymbol{\theta}_t)$ is actually beneficial for performance. The main difference occurs when a sign flip takes place due to the gradient step (that is, $\text{sign}(\boldsymbol{\theta}_{t+\frac{1}{2}}) \neq \text{sign}(\boldsymbol{\theta}_t)$), which can lead to a discrepancy in discrete time. Then, updating the sign leads to an acceleration away from zero, as the gradient $\nabla f(\boldsymbol{\theta}_t)$ does not change and still points in the same direction. This further aids in preventing parameters getting stuck at zero, apart from the benefits of the hyperbolic step on its own. We present the different cases in Figure 3.

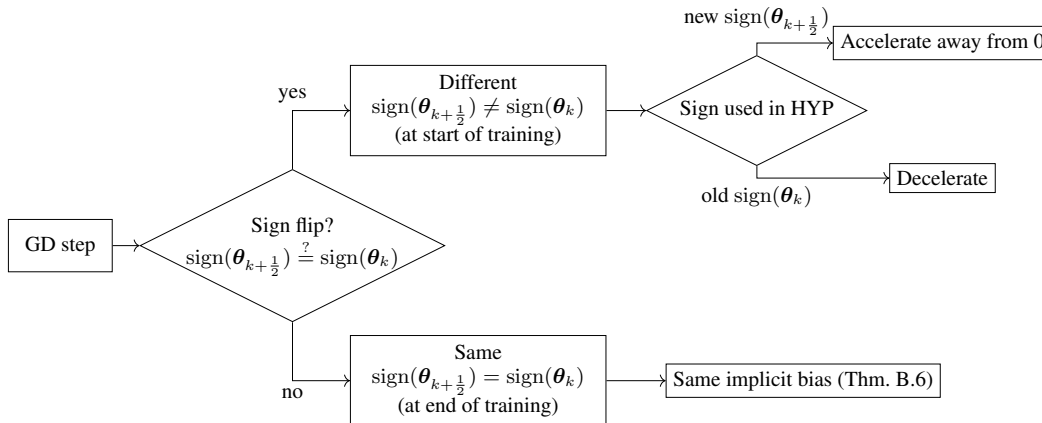


Figure 3: The difference between using $\text{sign}(\boldsymbol{\theta}_{k+\frac{1}{2}})$ and $\text{sign}(\boldsymbol{\theta}_k)$ in HYP. The main change we incur by using the new sign is that it accelerates away from zero when a sign flip occurs. Thus, when parameters are small, we can be more certain that they are actually redundant. Furthermore, when sign flips become less frequent due to decreasing learning rate at the end of training, we get the same implicit bias regardless, as shown in Theorem B.6.

E ONE-NEURON TOY EXAMPLE SIGN FLIPS

We show with a similar arguments as in (Gadhikar et al., 2025) that HAM allows for sign flips in a one neuron toy example. For this argument we similarly set $\beta = 0$ and we have to use a layerwise different α . In the same vein we argue that in presence of more overparameterization using the same α constant is fine. This is also empirically substantiated by observing more sign flips with HAM.

One dimensional neuron Consider a Gaussian i.i.d. data set $z_i \sim \mathcal{N}(0, 1)$ with $i \in [d]$. Let $f : \mathbb{R} \times \mathbb{R} \rightarrow \mathbb{R}$ be our objective function described by:

$$f(a, w) = \frac{1}{2d} \sum_{i=1}^d (y_i - a\sigma(wz_i))^2$$

where $\sigma(\cdot) = \max\{0, \cdot\}$ is the Rectified Linear Unit (ReLU). We want to learn a target one dimensional neuron $\tilde{a}\sigma(\tilde{w}\cdot)$, which generates the outputs y_i for $i \in [d]$. Then gradient flow dynamics for HAM is described by:

$$\begin{cases} da_t = -(\alpha_1|a_t| + 1) \partial_a f(a_t, w_t) dt, & a_0 = a_{\text{init}} \\ dw_t = -(\alpha_2|w_t| + 1) \partial_{w_1} f(a_t, w_t) dt, & w_0 = w_{\text{init}}. \end{cases} \quad (12)$$

Note that standard gradient flow would get stuck at zero, as it has to satisfy a balance equation in Lemma E.1, which is based on Theorem 2.1 in (Gadhikar et al., 2025). The balance equation implies that if $a_0^2 - w_0^2 = C$, then for all $t \geq 0$ we have that $a_t^2 - w_t^2 = C$ (In our case: $C = 0$). In order that the student with parameters (a, w) learn the ground truth, the parameters have to be able to sign flip when they don't match the ground truth's sign. This can be divided into four cases, i.e. the total amount of sign cases. In the balanced setting for gradient flow, the ground truth is recoverable only if the parameter signs align. Results of these four cases are shown in Figure 4.

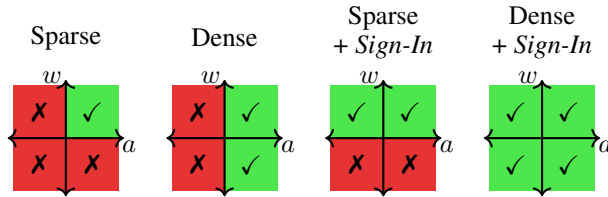


Figure 4: (Figure 2 from Gadhikar et al. (2025)), showing sign flipping benefits achieved with pointwise overparameterization $m \odot w$, for the sparse and dense case on a single-hidden neuron model.

Lemma E.1 Let $\tilde{g}(a, w) = \tilde{a}\sigma(\tilde{w}\cdot)$ with $\tilde{w} > 0$ be the teacher and f be the student network objective such that a and w follow the gradient flow dynamics in Eq. (12) with a random balanced parameter initialization. For $\alpha_1 = \alpha_2 = 0$ (standard gradient flow) the student only can learn one of four cases i.e. when $w_{\text{init}} > 0$ and $\text{sign}(a_{\text{init}}) = \text{sign}(\tilde{a})$.

Proof. If w_{init} is negative then it needs to flip its sign which is prevented by the ReLU activation. We know from the balance equation that for $t \geq 0$:

$$|a_t| = |w_t|.$$

This implies that if $a_t = 0$ then $w_t = 0$ implying we can also not recover the case where $\text{sign}(a_{\text{init}}) \neq \text{sign}(\tilde{a})$. \square

We now show that Eq. (12) can find the ground truth, even if the sign of a is misaligned, similarly as in (Gadhikar et al., 2025) for the $m \odot w$ reparameterization.

Theorem E.2 Let $\tilde{g}(a, w) = \tilde{a}\sigma(\tilde{w}\cdot)$ with $\tilde{w} > 0$ be the teacher and f be the student network objective such that a and w follow the gradient flow dynamics in Eq. (12) with a random balanced parameter initialization. Moreover, let $\alpha_1 > \alpha_2 > 0$. If $w_{\text{init}} > 0$, then f can learn the correct target with probability $1 - (\frac{1}{2})^d$. In the other case ($w_{\text{init}} \leq 0$) learning fails.

Proof. The proof idea is to show that for a balanced initialization with $w_{init} > 0$ the flow for $t > 0$ always enters the open set

$$\Gamma_0 := \{(a, w) \in \mathbb{R}^2 : a < -w, w > 0\}.$$

Furthermore, we show that the flow stays in the open set Γ_0 . The system is a Riemannian gradient flow which implies that the flow converges towards a stationary point in Γ_0 . It remains to be shown that the stationary point at the origin is a saddle and the stable manifold of the origin is not in Γ_0 . Thus, the remaining stationary points are the global optimizers.

First we show that for balanced initializations $|a_{init}| = w_{init} > 0$ enter the region Γ_0 , which can be divided into two cases. In case $a_{init} = w_{init} > 0$, we have $(a_{init}, w_{init}) \in \Gamma_0$. In case $-a_{init} = w_{init} > 0$, we have that $(a_{init}, w_{init}) \in \Gamma_0 \setminus \Gamma_0$ i.e. the boundary of Γ_0 . Therefore, we need to show the gradient field at (a_{init}, w_{init}) points into Γ_0 .

The balanced initialization implies that

$$\partial_a f(a_{init}, w_{init}) = -\partial_w f(a_{init}, w_{init}).$$

Moreover, since $\tilde{a} > 0$, $\partial_a f(a_{init}, w_{init}) > 0$. Using that $\alpha_1 > \alpha_2 > 0$ we have that the gradient field satisfies:

$$\begin{aligned} da_{init} &= -(\alpha_1 |a_{init}| + 1) \partial_a f(a_{init}, w_{init}) dt \\ &= (\alpha_1 |w_{init}| + 1) \partial_w f(a_{init}, w_{init}) dt \\ &< (\alpha_2 |w_{init}| + 1) \partial_w f(a_{init}, w_{init}) dt = -dw_{init} \end{aligned}$$

Therefore there is a $t_0 > 0$ such that $a_{t_0} < -w_{t_0} < 0$. Thus there is a $t_0 > 0$ such that $(a_{t_0}, w_{t_0}) \in \Gamma_0$.

We have entered the set Γ_0 , we have to show that we cannot leave the set Γ_0 . This can be shown by computing the gradient field at the boundaries. The boundary can be split up into three cases:

- $B_1 := \{(a, w) \in \mathbb{R}^2 : -a = w > 0\}$
- $B_2 := \{(a, w) \in \mathbb{R}^2 : w = 0, a > 0\}$
- The origin $\{(0, 0)\}$

The first case of B_1 is covered by the balanced initialization. For the second case of B_2 we can compute the gradient field again. We now only need that $dw_t > 0$. We linearize dw_t :

$$dw_t = Ca_t dt > 0,$$

where $C = \frac{1}{d} \sum_{i=1}^d \max\{0, z_i\}^2 > 0$ with probability $1 - (\frac{1}{2})^d$. The last case is the saddle point at the origin which we show is not possible to be reached from the open set Γ_0 . Thus for all $(a_{init}, w_{init}) \in \Gamma_0$ we have that for all $t \geq 0$, $(a_t, w_t) \in \Gamma_0$ or $\lim_{t \rightarrow \infty} (a_t, w_t) = (0, 0)$.

In the case that $w > 0$ the flow can be written as a dynamical system on a Riemannian manifold. This allows us to guarantee convergence to a stationary point. The flow is given by

$$\begin{cases} da_t = -C(\alpha_1 |a_t| + 1)(a_t w_t^2 - w_t) dt & a_0 = a_{init} \\ dw_t = -C(\alpha_2 |w_t| + 1)(a_t^2 w_t - a_t) dt & w_0 = w_{init}, \end{cases}$$

where $C = \frac{1}{d} \sum_{i=1}^d \max\{0, z_i\}^2 > 0$ with probability $1 - (\frac{1}{2})^d$. This dynamical system has stationary points at the origin and the set $aw = 1$. The dynamical system is a Riemannian gradient flow system therefore the flow converges to a stationary point. The stationary point at the origin is a saddle point. Therefore, the only way of getting stuck at the origin is when we initialize on the associated stable manifold. We show that this not possible for the balanced initialization. We calculate the linearization of the stable manifold and use that the balanced initialization stays in Γ_0 . The linearization at the origin $(0, 0)$ is given by

$$\begin{cases} da_t = Cw_t dt \\ dw_t = Ca_t dt. \end{cases}$$

By a direct calculation of the eigen vectors the linearization of the stable manifold is given by the vector $(-1, 1)$. This is the exact boundary of Γ_0 , for which we showed that for finite w_{init} and a_{init}

we enter Γ_0 . Suppose that from Γ_0 the stable manifold is reachable. Then there is a continuous differentiable curve γ_t with initialization $\gamma_0 = (a_{init}, w_{init}) \in \Gamma_0$ such that $\lim_{t \rightarrow \infty} \gamma_t = (0, 0)$. This is not possible as it violates the gradient field at the boundaries of Γ_0 . Thus, the flow does not converge to the stationary point at the origin. This concludes the first part, since the only set of stationary points are the set of global optima.

The other two remaining cases fail as the boundary at $w = 0$ is not differentiable and the gradient flow stops there. \square

Theorem E.2 highlights a benefit of HAM over gradient flow. A key difference with the proof in (Gadhikar et al., 2025) is that now the stable manifold is exactly the boundary at Γ_0 . Therefore, we are relying on the non-linearity of the model to push us into the open set Γ_0 . A similarity between the proofs is that we rely on $\alpha_1 > \alpha_2 > 0$. In the next part we argue that for multidimensional inputs this is not necessary and we can use a single constant α .

Multidimensional neuron We can consider the gradient field at a balanced initialization for a multidimensional input case. Then we have the following inequality:

$$(\alpha|a_{init}| + 1) = (\alpha\|\mathbf{w}_{init}\|_{L_2} + 1) \geq \frac{1}{\sqrt{n}} (\alpha\|\mathbf{w}_{init}\|_{L_1} + 1) \geq \frac{1}{n} \sum_{i=1}^n (\alpha|w_{in,i}| + 1) \quad (13)$$

where we used the relation between the L_1 and L_2 norm. Note that now there is a significant gap due to switching between \sqrt{n} and n . This inequality ensures that at initialization the gradient field is pointing in a similar direction as for the one dimensional case, promoting useful sign flips (Gadhikar et al., 2025).

F ILLUSTRATION OF VANISHING INVERSE METRIC

We track the average inverse metric coefficient at $\theta = \mathbf{0}$. This implies for HAM we get $g^{-1}(\mathbf{0}) = 1$ by definition of its inverse metric. For $m \odot w$ we get $g^{-1}(\mathbf{0}) = m^2 - w^2$. We track the average during training in the first layer of a ResNet50 trained on Imagenet. We consider 4 scenarios: HAM, Sign-In for 90% sparsity according to (Gadhikar et al., 2025), dense training $m \odot w$ with and without weight decay. The weight decay selected for $m \odot w$ is set to $2e - 5$, which is less than half of the strength it would be in case of dense training. Note that in both cases a Frobenius decay i.e. $\|m \odot w\|_{L_2}^2$ is applied in accordance with (Jacobs & Burkholz, 2025).

In Figure 5 we observe that the inverse metrics of $m \odot w$ decays severely when weight decay is applied. For the reparameterization, weight decay is needed to induce sparsity, so in order to use it for sparsity it needs to be used. Furthermore, note that even though Sign-In manually resets the rescaling at the start of training the metric decays at the end of training.

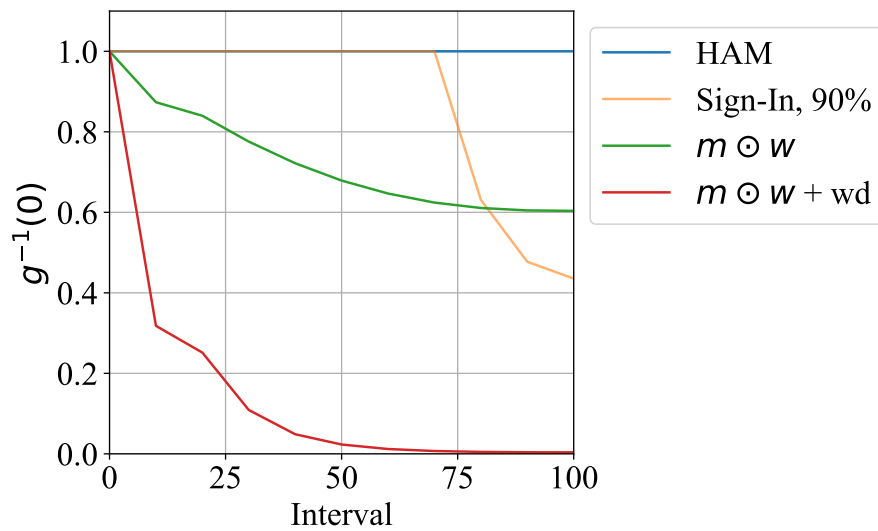


Figure 5: The first layer of a Resnet50’s average inverse metric at zero reported at every tenth epoch.

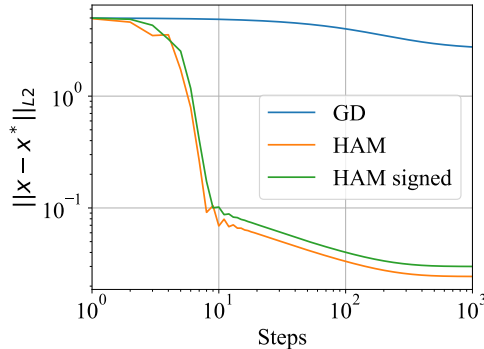


Figure 6: Gradient flow simulation of HAM, HAM with corrected sign and gradient descent. Observe the slight benefit of using $\text{sign}(\theta_{k+\frac{1}{2}})$ instead of $\text{sign}(\theta_k)$.

G EXPERIMENTAL DETAILS

We present the additional hyper parameters and other details of the experimental setup. Furthermore we provide ablations on various setups. In general HAM is applied to all layers except the batchnorm or layernorm layers.

G.1 OVERPARAMETERIZED LINEAR REGRESSION

We illustrate Theorem 4.5 by considering a under-determined linear regression setup, similar to that of Pesme et al. (2021); Jacobs & Burkholz (2025). We consider a sparse groundtruth θ^* and initialize at $\theta_0 = \mathbf{0}$. Moreover, we use the mean squared error loss function. We generate data by sampling $z_i \sim \mathcal{N}(\mathbf{0}, \mathbf{I})$ i.i.d. for $i \in [d]$, with $d = 40$ and $n = 100$. We compare gradient descent with and without HAM. Moreover we also show what happens if we replace $\text{sign}(\theta_{k+\frac{1}{2}})$ with $\text{sign}(\theta_k)$ denoted with HAM signed. The learning rate is set $\eta = 10^{-4}$, and both algorithms are run for $10e + 6$ steps. We track the distance to the ground truth during training. In Figure 6 we observe that HAM gets closer to the ground truth and converges faster then both gradient descent and HAM signed, where we set $\alpha = 1000$. This corresponds to a less strong sparse implicit bias than L_1 .

In the same setting, we illustrate why we need both steps (GD;HYP*). We do this with an ablation, i.e., by using the hyperbolic step (HYP*) and gradient descent (GD) on their own. We initialize $\epsilon = -10e - 5 \cdot \mathbf{1}$. This means we initialize with the opposite signs compared with the ground truth. In Figure 7, we observe that HAM reaches close to the ground truth, while the exponential step diverges, as it can not reach the ground truth due to having no sparse implicit bias. Moreover, gradient descent can also not reach the ground truth on its own. Therefore, both the hyperbolic and the gradient steps are necessary.

Furthermore, if we increase α and decrease the learning rate η , we can recover the ground truth solution. Concretely, consider HAM with the following configurations $(\alpha, \eta) = (10^{3+j}, 10^{-4-j})$ for $j \in [3]$. In Figure 8, we observe that we get closer to the ground truth.

G.2 DENSE AND SPARSE TRAINING ON VISION TASKS AND ABLATION

We provide additional results on CIFAR100 (Krizhevsky et al., 2009) in Table 7. Furthermore, we train a small DeiT (Touvron et al., 2021) with AdamW in Table 8. All results are for 3 seeds. We provide the hyperparameter grid search for CIFAR 100 and Imagenet (Deng et al., 2009) in Figures 11 and 12. We find that the grid search is consistent i.e. there is a global best configuration. This implies it is easy to tune for specific tasks. We illustrate the convergence and implicit bias behaviour by tracking the training loss and L_1 norm in Figure 9. We also track the L_1 norm when comparing with SAM to show that SAM and HAM exploit different principles in Figure 10. The additional hyper-parameters of the experiments can be found in Table 5. The same parameters are used for the

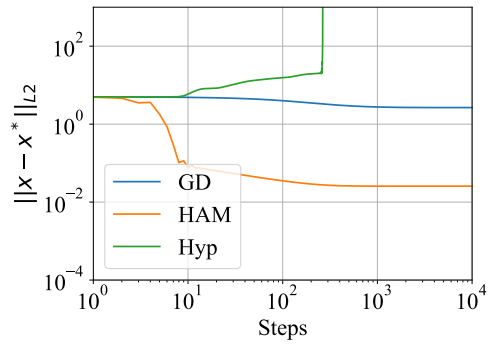


Figure 7: HAM vs hyperbolic step (HYP*) under the incorrect sign initializations.

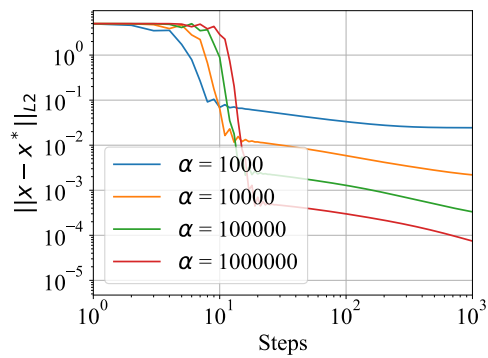


Figure 8: Gradient flow simulation of HAM with corrected sign for different α . Larger α leads to closer ground truth recovery.

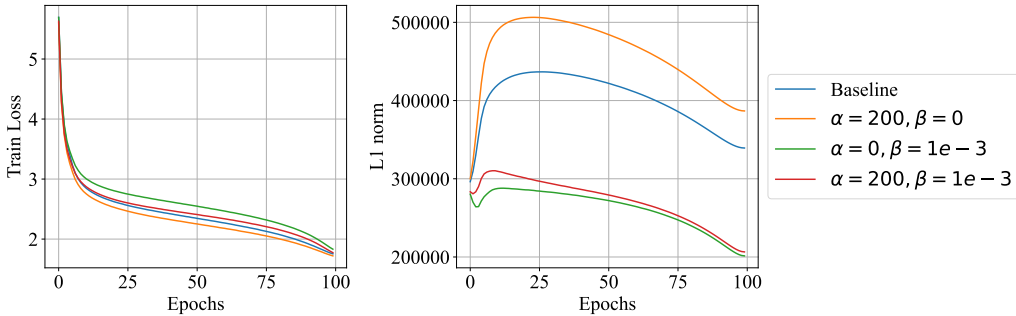


Figure 9: Training dynamics of HAM compared to the baseline for a ResNet 50 on Imagenet. Observe in the first figure (left) that the average training loss converges faster with higher α given the same β . This illustrates the convergence speed up predicted by our developed theory. Moreover, in the second figure (right) the average L_1 norm decays more due the regularization constant β , whereas larger α leads to a larger initial increase in the average L_1 norm it decays faster in the end. This is in line with being more uncertain about the sign of the weights in the beginning of training.

sparse training setup. To reproduce sparse training methods including AC/DC, RiGL and STR we use hyperparameters prescribed by the authors. Each experiment was run on 4 A100 GPUS. The code used is based on TurboPrune as in (Nelaturu et al.).

Parameters for $m \odot w$ The $m \odot w$ parameterization is not regularized with weight decay for the dense scenario, as this induces sparsity. Instead, weight decay is applied on the product $\|m \odot w\|_{L_2}^2$ with strength $5e - 5$, the same strength as for dense training (Gadhikar et al., 2025).

HAM optimization To optimize with HAM for dense and sparse training setups on vision tasks, we use $\alpha = 200$ and $\beta = 1e - 3$ based on our grid search in Figure 12. Additionally, we clamp the exponent in the HAM step (see Equation HYP*) between $[-5, 5]$ to avoid exploding gradients. Note, in all experiments, (HYP*) is not applied to BatchNorm or LayerNorm layers.

Table 5: Training Details for the dense vision experiments presented in the paper.

Dataset	Model	LR	Weight Decay	Epochs	Batch Size	Optim	LR Schedule
CIFAR100	ResNet18	0.2	$1e - 4$	150	512	SGD, $m = 0.9$, SAM	Triangular
ImageNet	ResNet50	0.25	$5e - 5$	100, 200	1024	SGD, $m = 0.9$, SAM	Triangular
	DeiT Small	0.005	$1e - 1$	300	1024	AdamW	Triangular

Table 6: HAM improves dense training of a ResNet50 on Imagenet (Deng et al., 2009).

Dataset	Baseline (no HAM)	$\alpha = 0, \beta = 1e - 3$	$\alpha = 200, \beta = 0$	$\alpha = 200, \beta = 1e - 3$
HAM, 100 epchs	76.72 ± 0.19	77.01 ± 0.14	76.72 ± 0.07	77.51 ± 0.11
HAM, 200 epchs	77.27 ± 0.13	77.48 ± 0.09	77.24 ± 0.09	77.86 ± 0.05
SAM-HAM, 100 epchs	77.10 ± 0.21	77.53 ± 0.16	77.21 ± 0.09	77.92 ± 0.15
SAM-HAM, 200 epchs	77.94 ± 0.16	78.17 ± 0.16	77.60 ± 0.03	78.56 ± 0.12

Table 7: Dense training with HAM on the CIFAR100 vision benchmarks.

Dataset	Baseline	$\alpha = 0, \beta = 16e - 3$	$\alpha = 200, \beta = 0$	$\alpha = 200, \beta = 16e - 3$
HAM	75.25 ± 0.24	75.36 ± 0.04	75.31 ± 0.30	76.12 ± 0.27
SAM-HAM	75.12 ± 0.68	76.30 ± 0.11	75.25 ± 0.20	76.65 ± 0.23

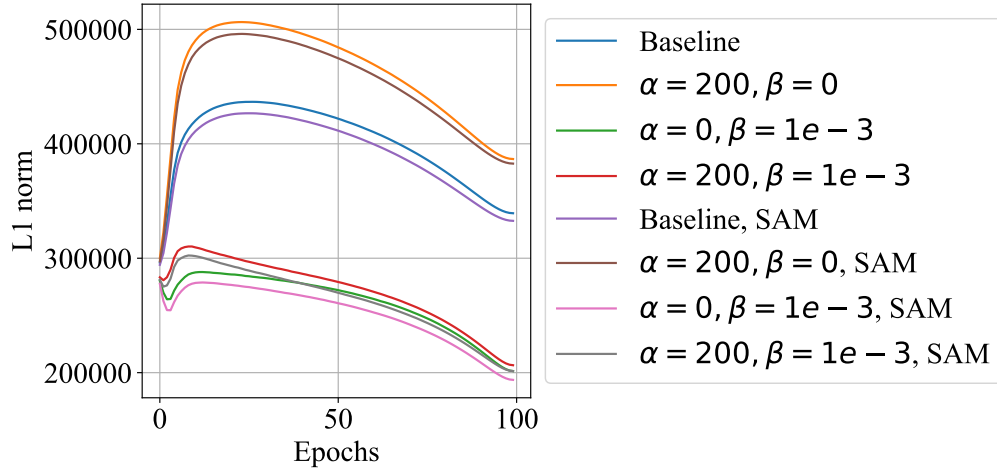


Figure 10: Training dynamics of HAM with and without SAM for a ResNet50 on Imagenet. Observe that the choice of our hyperparameters α and β determine the general trend of the average L_1 norm while the choice between SGD and SAM make less of a difference. This provides additional evidence for their complementary working.

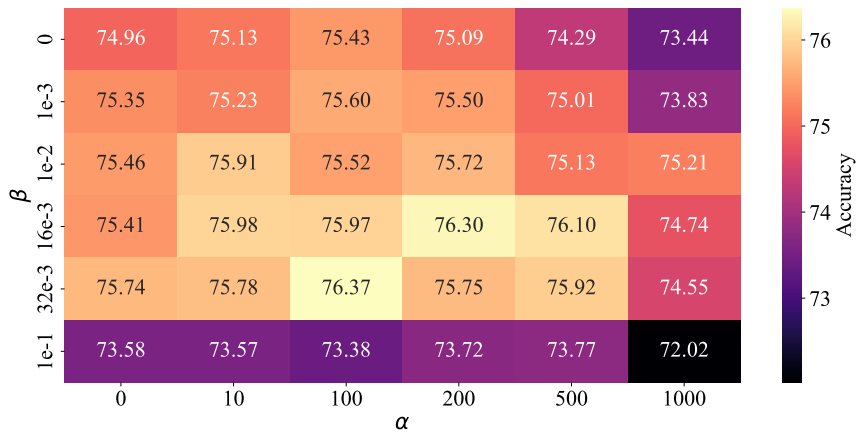


Figure 11: One seed hyperparameter search for a ResNet18 on CIFAR100.

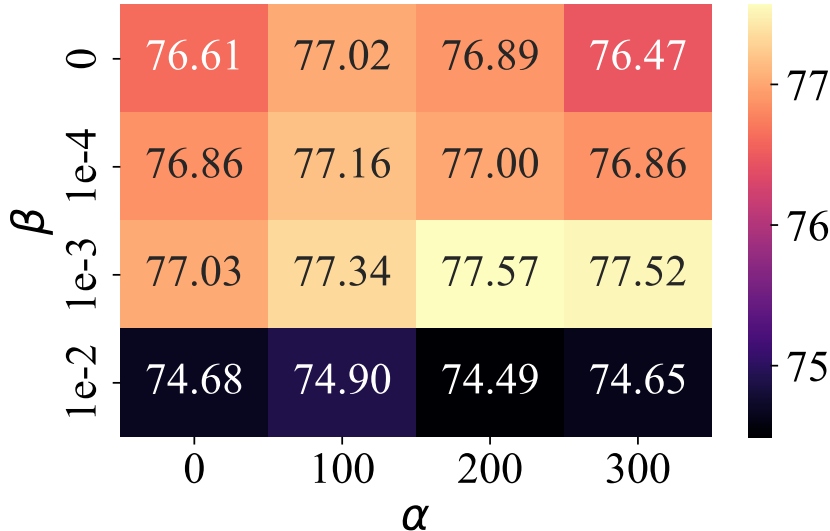


Figure 12: One seed hyperparameter search for a Resnet 50 on Imagenet.

G.3 HAM FOR VISION TRANSFORMERS

We also verify that HAM can boost pre-training performance for ViTs trained with AdamW, for both dense training as well as sparse training with AC/DC as shown in Table 8 and Table 9 respectively. We use the same hyperparameters as for the ResNet-50 trained on Imagenet: $(\alpha, \beta) = (200, 1e - 3)$.

Table 8: Pre-training a vision transformer from scratch for 300 epochs on ImageNet.

Setup	AdamW + HAM	AdamW
ImageNet+ DeiT Small	72.62\pm0.22	72.31 \pm 0.09

Table 9: Sparse pre-training of a vision transformer with AC/DC for 300 epochs on ImageNet at 50% sparsity.

Setup	AC/DC + HAM	AC/DC
ImageNet+ DeiT Small	73.24\pm0.45	72.5 \pm 0.16

G.4 TRAINING WITH HAM AND DIFFERENT SPARSE MASKS.

HAM can be used to optimize sparse networks with different mask topologies. We train the nonzero weights of sparse mask topologies identified by different sparse methods including AC/DC, RiGL, STR and PaI masks. The weights are randomly initialized and optimized with HAM.

Note, this is equivalent to pruning at initialization with the mask obtained from the listed methods. We see a consistent improvement across all topologies with HAM except the SNIP mask, which was unstable to train also without HAM. HAM performs best for sparse masks identified by RiGL and random pruning, potentially due to better trainability and good layerwise sparsity ratios identified by these methods, which influences performance when the mask does not change during training. Results are provided in Table 10.

Table 10: HAM with different masks for a ResNet50 trained on ImageNet with 90% sparsity and random initialization. (* denotes a single run, as the runs for other seeds crashed.)

Mask	Init		
	Base	<i>Sign-In</i>	HAM
AC/DC	70.66 \pm 0.12	70.96 \pm 0.09	71.84 \pm 0.17
RiGL	72.02 \pm 0.23	72.48 \pm 0.19	73.31 \pm 0.01
STR	68.36 \pm 0.17	67.81 \pm 0.34	68.75 \pm 0.16
Snip	52.9*	54.27*	44.48 \pm 0.57
Synflow	60.66 \pm 0.2	60.59 \pm 0.07	62.4 \pm 0.03
Random	71.56 \pm 0.03	72.19 \pm 0.18	72.72 \pm 0.03

G.5 PRUNING DENSE MODELS

Here we magnitude prune the best dense models acquired from both HAM and standard training. We observe in Table 11 that HAM’s implicit sparsity bias makes the model perform relatively better than the standard dense model.

Table 11: Validation accuracy comparison between Pruned HAM and Dense models at different sparsity levels.

Sparsity	HAM	Dense
0.9	1.384	0.104
0.8	59.008	0.424
0.7	71.940	37.776
0.5	76.824	73.404

G.6 FINETUNING LLMs

As we show, HAM can also boost the performance of LLM finetuning. We evaluate on the commonsense reasoning benchmark (Hu et al., 2023) to finetune LLaMA 3.2 models (Grattafiori et al., 2024) and report accuracies across eight benchmarks in Table 12. On average, HAM improves on this task, demonstrating its compatibility with the optimizer ADAM and the LoRA architecture.

Table 12: Performance of LoRA + HAM on the commonsense reasoning (Hu et al., 2023) benchmark.

LlaMa 3.2	Size	HS	WG	PQ	AE	AC	OB	SQ	BQ	Avg
LoRA	1B	63.8	65.8	74.04	67.63	55.88	63.6	70.98	64.25	65.74
LoRA + HAM	1B	64.8	68.35	74.21	68.39	51.79	65.8	71.2	62.17	65.83
LoRA	3B	88.8	80.66	83.73	82.65	66.89	76.8	78.19	69.44	78.39
LoRA + HAM	3B	89.40	80.58	82.69	81.77	68.43	80.2	78.25	69.48	78.85

Experimental details Each experiment was run on 4 A100 GPUs. We use the experimental setup of DoRA Liu et al. (2024) to finetune LLaMA 3.2 models of size 1B and 3B with $\alpha = 200, \beta = 1e-3$ and $\alpha = 100, \beta = 1e-4$ respectively. We find that larger models benefit from less strong regularization which is consistent with our different regularization strengths β for ResNet18 and ResNet50.

G.7 GRAPH AND NODE CLASSIFICATION

We report the experimental details of the 4 graph classification benchmarks from Table 13. We also include results on 13 node classification benchmarks, and an ablation on $\alpha < 0$. Each experiment was run on an A100. We consider 4 graph classification tasks on the GCN architecture (Kipf & Welling, 2017) in Table 13, and 13 node classification tasks on GCN, GATv2 (Brody et al., 2022), and GraphSAGE (Hamilton et al., 2017) in Tables 15, 16. We also include the hyperparameter grid search, as well as an ablation on negative α . The success of negative values indicates that node classification prefers a different type of implicit bias. Nonetheless, we see consistent improvements across almost all datasets and architectures with $\alpha > 0$.

Table 13: Evaluation of HAM on 4 graph classification benchmarks from OGB (Hu et al., 2020).

Dataset	ogbg-ppa	ogbg-molpcba	ogbg-molhiv	ogbg-code2
Metric	Accuracy \uparrow	Avg. Precision \uparrow	AUROC \uparrow	F1 score \uparrow
GCN	75.48 \pm 0.15	27.57 \pm 0.04	82.37 \pm 0.29	13.89 \pm 2.11
GCN + HAM	75.72 \pm 0.24	27.81 \pm 0.22	82.50 \pm 0.69	13.96 \pm 2.06

G.7.1 GRAPH CLASSIFICATION

We report the performance of HAM on four graph classification datasets from Open Graph Benchmark (OGB) (Hu et al., 2020). The code to run these benchmarks is based on (Luo et al., 2025), using their choice of hyperparameters and ADAM as the optimizer. We use their GCN+ architecture, which is a GCN equipped with edge features, normalization, dropout, residual connections, feed-forward networks, and positional encodings. In order to implement HAM in combination with dropout, we mask the regularization term β with ($\text{grad} \neq 0$). We only apply HAM on the weights and biases associated with the convolutional layers. The results, shown in Table 13, are averaged over 3 seeds. We report the best validation metric for the best values of α and β for HAM, the selection of which is displayed in Table 14. The tuning range is $\alpha \in \{1, 10, 100, 200\}$, and $\beta \in \{0, 0.01, 0.1\}$. Table 14 also includes the size of the datasets in terms of number of graphs. Note that for three datasets, α is the same as for the vision tasks.

Table 14: α and β best values for the graph classification tasks.

Dataset	ogbg-ppa	ogbg-molpcba	ogbg-molhiv	ogbg-code2
# graphs	158,100	437,929	452,741	41,127
α	200	200	200	1
β	0.1	0.1	0.1	0.01

G.7.2 NODE CLASSIFICATION

We furthermore report the performance of HAM on thirteen node classification datasets: Cora, CiteSeer, and PubMed (Kipf & Welling, 2017), Wiki-CS (Mernyei & Cangea, 2022), Coauthor-CS, Coauthor-Physics, Amazon-Computers, and Amazon-Photo (Shchur et al., 2019) (homophilic); Amazon-Ratings, Squirrel, Chameleon, Minesweeper, and Roman-Empire (Platonov et al., 2023) (heterophilic). We evaluate over GCN, GATv2, and GraphSAGE. We only apply HAM on the weights and biases associated with the convolutional layers and on the attention parameters. The code to run these benchmarks is based on (Luo et al., 2024), using their choice of hyperparameters and ADAM as the optimizer. The results, shown in Tables 15 (homophilic) and 16 (heterophilic), are averaged over different runs according to the original setup. We report the best validation accuracy for the best values of α and β for HAM, the selection of which is displayed in Table 17. The tuning range is $\alpha \in \{1, 10, 100, 200\}$, and $\beta \in \{0, 0.01, 0.1\}$. The best value per architecture is in bold, and ties are underlined. Tables 15 and 16 also include the size of the datasets in terms of number of nodes and edges.

Table 15: Evaluation of HAM on 8 homophilic node classification benchmarks.

Dataset	cora	citeseer	pubmed	wikis	coauthor-cs	coauthor-physics	amazon-computer	amazon-photo
# nodes	2,708	3,327	19,717	11,701	18,333	34,493	13,752	7,650
# edges	5,278	4,522	44,324	216,123	81,894	247,962	245,861	119,081
GCN	81.32 ± 0.30	68.60 ± 0.94	77.96 ± 0.46	80.71 ± 0.29	95.32 ± 0.12	97.17 ± 0.01	83.47 ± 0.70	94.33 ± 0.61
GCN+HAM	81.44 ± 0.43	68.64 ± 0.97	78.16 ± 0.65	80.84 ± 0.27	95.32 ± 0.04	97.18 ± 0.02	83.93 ± 0.58	95.33 ± 0.23
GAT	81.24 ± 0.68	68.68 ± 0.30	79.00 ± 0.95	82.35 ± 0.39	95.33 ± 0.07	97.15 ± 0.01	83.67 ± 0.23	94.47 ± 0.31
GAT+HAM	81.56 ± 0.67	68.92 ± 0.27	79.08 ± 0.88	82.47 ± 0.38	95.33 ± 0.07	97.16 ± 0.01	84.40 ± 0.92	94.60 ± 0.69
SAGE	80.44 ± 1.03	67.44 ± 0.26	79.36 ± 0.67	81.72 ± 0.46	95.50 ± 0.08	97.01 ± 0.10	83.07 ± 0.90	95.33 ± 0.31
SAGE+HAM	80.60 ± 0.63	67.48 ± 0.18	79.96 ± 0.62	81.78 ± 0.41	95.58 ± 0.09	97.03 ± 0.08	83.60 ± 1.11	95.40 ± 0.40

Table 16: Evaluation of HAM on 5 heterophilic node classification benchmarks.

Dataset	amazon-ratings	squirrel	chameleon	minesweeper	roman-empire
# nodes	24,492	2,223	890	10,000	22,662
# edges	93,050	46,998	8,854	39,402	32,927
GCN	53.23 ± 0.54	44.52 ± 1.12	46.12 ± 2.38	97.46 ± 0.24	90.96 ± 0.33
GCN+HAM	53.43 ± 0.44	44.55 ± 1.28	46.78 ± 2.22	97.78 ± 0.53	91.22 ± 0.40
GAT	55.47 ± 0.20	42.22 ± 1.73	45.84 ± 3.02	97.98 ± 0.21	90.58 ± 0.91
GAT+HAM	55.58 ± 0.47	43.17 ± 1.37	46.37 ± 3.32	98.37 ± 0.46	90.83 ± 0.89
SAGE	55.05 ± 0.50	40.91 ± 1.27	42.80 ± 2.90	97.02 ± 0.59	90.51 ± 0.33
SAGE+HAM	55.50 ± 0.55	40.85 ± 1.16	43.07 ± 2.84	97.77 ± 0.16	90.57 ± 0.44

Table 17: α and β best values for the node classification tasks.

Dataset ↓	GCN		GAT		SAGE	
	α	β	α	β	α	β
cora	200	0.1	200	0.1	200	0.1
citeseer	1	0.01	10	0	200	0.01
pubmed	200	0.1	100	0	10	0.01
wikis	10	0.01	1	0.1	1	0.1
coauthor-cs	1	0.1	10	0.1	10	0.1
coauthor-physics	10	0	10	0.01	1	0
amazon-computer	10	0.01	10	0	200	0
amazon-photo	10	0.01	10	0	1	0.01
amazon-ratings	10	0.01	200	0.01	200	0
squirrel	10	0.01	200	0	200	0.1
chameleon	200	0	200	0	200	0.1
minesweeper	200	0.1	100	0.1	1	0.01
roman-empire	10	0.1	10	0.1	10	0.1

Node classification with $\alpha < 0$ We perform an ablation on the node classification tasks by assigning negative values to α , denoted as nHAM. Tables 18 (homophilic) and 19 (heterophilic) show the results of this ablation, while Table 20 displays the optimal pair of $(\alpha < 0, \beta)$ hyperparameters. Note that the baselines never perform better than HAM or nHAM. Surprisingly, heterophilic datasets appear to be able to benefit more consistently from nHAM, especially for GCN and GraphSAGE. In homophilic datasets and GATs, it still provides consistent but smaller improvements, or matches the best performance of $\alpha > 0$. This intriguing phenomenon requires further investigation, as it may indicate the need for a different kind of implicit bias in certain graph-based architectures. Other methods particularly effective in heterophilic settings, such as modifying the adjacency matrix (Qian et al., 2024; Jamadandi et al., 2024; Rubio-Madrigal et al., 2025), may offer insight into these results.

Table 18: HAM ($\alpha > 0$) compared to nHAM ($\alpha < 0$) on 8 homophilic node classification benchmarks.

Dataset	cora	citeseer	pubmed	wikics	coauthor-cs	coauthor-physics	amazon-computer	amazon-photo
GCN	81.32 ± 0.30	68.60 ± 0.94	77.96 ± 0.46	80.71 ± 0.29	95.32 ± 0.12	97.17 ± 0.01	83.47 ± 0.70	94.33 ± 0.61
GCN+HAM	81.44 ± 0.43	68.64 ± 0.97	78.16 ± 0.65	80.84 ± 0.27	95.32 ± 0.04	97.18 ± 0.02	83.93 ± 0.58	95.33 ± 0.23
GCN+nHAM	<u>81.44 ± 0.26</u>	68.68 ± 0.99	78.08 ± 0.58	80.89 ± 0.30	95.34 ± 0.09	97.17 ± 0.00	84.20 ± 0.40	95.27 ± 0.50
GAT	81.24 ± 0.68	68.68 ± 0.30	79.00 ± 0.95	82.35 ± 0.39	<u>95.33 ± 0.07</u>	97.15 ± 0.01	83.67 ± 0.23	94.47 ± 0.31
GAT+HAM	81.56 ± 0.67	68.92 ± 0.27	79.08 ± 0.88	82.47 ± 0.38	<u>95.33 ± 0.07</u>	97.16 ± 0.01	84.40 ± 0.92	94.60 ± 0.69
GAT+nHAM	<u>81.56 ± 0.43</u>	<u>68.92 ± 0.18</u>	<u>79.08 ± 0.88</u>	82.45 ± 0.41	<u>95.33 ± 0.07</u>	<u>97.16 ± 0.01</u>	83.93 ± 0.31	94.80 ± 0.72
SAGE	80.44 ± 1.03	67.44 ± 0.26	79.36 ± 0.67	81.72 ± 0.46	95.50 ± 0.08	97.01 ± 0.10	83.07 ± 0.90	95.33 ± 0.31
SAGE+HAM	80.60 ± 0.63	67.48 ± 0.18	79.96 ± 0.62	81.78 ± 0.41	95.58 ± 0.09	97.03 ± 0.08	83.60 ± 1.11	95.40 ± 0.40
SAGE+nHAM	81.00 ± 0.35	<u>67.48 ± 0.23</u>	79.84 ± 0.93	81.82 ± 0.45	95.56 ± 0.12	97.02 ± 0.10	<u>83.60 ± 1.04</u>	95.67 ± 0.61

Table 19: HAM ($\alpha > 0$) compared to nHAM ($\alpha < 0$) on 5 heterophilic node classification benchmarks.

Dataset	amazon-ratings	squirrel	chameleon	minesweeper	roman-empire
GCN	53.23 ± 0.54	44.52 ± 1.12	46.12 ± 2.38	97.46 ± 0.24	90.96 ± 0.33
GCN+HAM	53.43 ± 0.44	44.55 ± 1.28	46.78 ± 2.22	97.78 ± 0.53	91.22 ± 0.40
GCN+nHAM	<u>53.43 ± 0.25</u>	44.58 ± 1.09	<u>46.78 ± 1.85</u>	97.85 ± 0.10	91.23 ± 0.36
GAT	55.47 ± 0.20	42.22 ± 1.73	45.84 ± 3.02	97.98 ± 0.21	90.58 ± 0.91
GAT+HAM	55.58 ± 0.47	43.17 ± 1.37	46.37 ± 3.32	98.37 ± 0.46	90.83 ± 0.89
GAT+nHAM	55.76 ± 0.55	42.84 ± 1.25	46.23 ± 2.91	98.53 ± 0.25	90.74 ± 0.82
SAGE	55.05 ± 0.50	40.91 ± 1.27	42.80 ± 2.90	97.02 ± 0.59	90.51 ± 0.33
SAGE+HAM	55.50 ± 0.55	40.85 ± 1.16	43.07 ± 2.84	97.77 ± 0.16	90.57 ± 0.44
SAGE+nHAM	55.25 ± 1.00	41.11 ± 1.61	43.32 ± 2.92	97.81 ± 0.14	90.64 ± 0.56

Table 20: α and β best values for the node classification tasks with $\alpha < 0$.

Dataset ↓	GCN		GAT		SAGE	
	α	β	α	β	α	β
cora	-10	0.01	-10	0	-200	0.01
citeseer	-1	0.01	-10	0	-100	0
pubmed	-100	0.01	-100	0	-1	0.1
wikics	-100	0.1	-10	0.01	-10	0.01
coauthor-cs	-10	0.01	-100	0.01	-100	0.01
coauthor-physics	-1	0.1	-1	0.01	-100	0.1
amazon-computer	-200	0	-1	0.01	-1	0.01
amazon-photo	-200	0	-200	0	-1	0.01
amazon-ratings	-10	0	-200	0.1	-1	0
squirrel	-100	0	-200	0.01	-200	0.1
chameleon	-200	0	-100	0	-200	0.1
minesweeper	-100	0.1	-10	0.1	-200	0.1
roman-empire	-200	0.1	-10	0.1	-1	0.1